J., Sundar, B.Tech., Indian Institute of Technology, Madras, 1984
Master of Science in Nuclear Engineering, Spring Commencement, 1989
Major: Nuclear Engineering
Radiative Transfer in Participating Media with Arrhenius Heat Gereration
Thesis directed by Associate Professor Adnan Yucel
Pages in Thesis, 90. Words in Abstract, 300.

ABSTRACT

The radiative transfer problem in pulverized coal combustion is described and a model is developed for solving the radiative transfer equation in nongray media in planar and cylindrical geometries. The multigroup formulation is adopted for discretizing the wavelength variable. A diffusion limited Arrhenius heat generation is used to describe the heat generation rate due to the oxidation of the coal particles. The particles in suspension in the medium are assumed to be bounded by black walls at constant temperature. A distribution of particle sizes is assumed and the Mie theory is applied to arrive at the spectral interaction coefficients. A FORTRAN code is developed to solve iteratively the system of coupled nonlinear equations describing radiative transfer and the internal heat generation in the medium.

The code is applied to study the effect of radiative heat transfer on thermal ignition of pulverized coal suspensions. A calculational model is presented for predicting ignition in coal dusts and particle suspensions. The P-3 spherical harmonics method is applied for the first time to predict radiative heat transfer in nongray planar and nonplanar enclosures with a range of particle sizes. This method has been extensively applied in neutron flux calculations in nuclear systems. The effect of the activation energy, optical thickness and the spectral

properties of the particles on the temperature and the critical heat generation rates (Hc) are determined.

Ignition is observed to occur only when the activation energy is greater than a critical value which lies between 7 and 8. This is consistent with earlier investigations. It is found that the treatment of nongray media in terms of an equivalent gray model underestimates the temperature by upto about 12 percent in both planar and cylindrical enclosures, and to predict ignition at higher Hc values- by about 35 to 39 percent for both geometries.

RADIATIVE TRANSFER IN PARTICIPATING MEDIA WITH ARRHENIUS HEAT GENERATION

A Thesis

Submitted to the Graduate Faculty of the
Louisiana State University and
Agricultural and Mechanical College
in partial fulfillment of the
requirements for the degree of
Master of Science in Nuclear Engineering

in

The Department of Nuclear Science

by
J., Sundar
B. Tech., Indian Institute of Technology, Madras, INDIA, 1984
May 1989

to my loving parents and
sisters Latha and Geetha

ACKNOWLEDGEMENTS

I would like to thank Dr. Adnan Yucel for his continued guidance and advice which have been of invaluable help in the completion of my thesis. I also wish to thank Dr. Mark Williams for all that he has taught me in the field of Nuclear Engineering. I would like to thank the Nuclear Science Center for the financial support provided to me during the course of my graduate studies. My thanks to Dr. Jack Courtney for continuing to support me in my final semester.

I convey my gratitude to Dr. Tryfon Charalampopoulos for sitting in my thesis defense.

My gratitude is extended to Yvonne Thomas for all the help given to me in preparing my thesis. I am especially thankful to her, and also to Kerry and Lana for their cheerfulness and amiability which made my stay here pleasant despite the many hardships I faced, especially towards the end of my degree program.

I thank Richard Teague from whom I have learned so much about computers.

My special and personal thanks to Dr. Edward Lambremont for giving me an opportunity to come here for pursuing graduate studies.

My infinite gratitude to my family members for their patience and encouragement.

TABLE OF CONTENTS

LIST OF TABLES

LIST OF FIGURES

NOMENCLATURE

A	pre-exponential factor in Arrhenius equation
D	particle diameter; the operator $d/d\tau$
E	activation energy
E_{bg}	normalized black body emissive power for group 'g'
H	Arrhenius heat generation rate
H_c	critical heat generation rate coefficient (critical A)
i_k	k'th moment of intensity
I_k	normalized moment of intensity
L	half dimension of the slab
l_r, l_η	direction cosines in cylindrical geometry
N	particle number density
NG	number of wavelength groups
q''_R	radiative heat flux
r	spatial variable in cylindrical geometry
R	radius of the cylinder; gas constant in Arrhenius equation
T_1, T_2	boundary temperatures in slab geometry
T_2	surface temperature in cylindrical geometry
T_r	reference temperature
z	spatial variable in slab geometry

GREEK SYMBOLS

α	non-dimensional activation energy
α_g	β_g/β_m

β_g	extinction coefficient for group 'g'
β_m	maximum extinction coefficient of all groups
κ_g	absorption coefficient for group 'g'
λ	wavelength variable
μ	direction cosine ($\cos\theta$) in slab geometry
$\hat{\sigma}$	Stefan-Boltzmann constant
σ_{sg}	scattering coefficient for group 'g'
τ	optical length ($z\beta_m$, $r\beta_m$)
τ_0	optical thickness ($2L\beta_m$ or $R\beta_m$)
$\hat{\Omega}$	direction vector in 3-dimensional space
θ	polar angle in slab and cylindrical geometry
Θ	dimensionless temperature (T/T_r)
Θ_1, Θ_2	normalized boundary temperatures in slab geometry
Θ_2	normalized surface temperature in cylindrical geometry
ω_g	scattering albedo (σ_{sg}/β_g)

ABSTRACT

The radiative transfer problem in pulverized coal combustion is described and a model is developed for solving the radiative transfer equation in nongray media in planar and cylindrical geometries. The multigroup formulation is adopted for discretizing the wavelength variable. A diffusion limited Arrhenius heat generation is used to describe the heat generation rate due to the oxidation of the coal particles. The particles in suspension in the medium are assumed to be bounded by black walls at constant temperature. A distribution of particle sizes is assumed and the Mie theory is applied to arrive at the spectral interaction coefficients. A FORTRAN code is developed to solve iteratively the system of coupled nonlinear equations describing radiative transfer and the internal heat generation in the medium.

The code is applied to study the effect of radiative heat transfer on thermal ignition of pulverized coal suspensions. A calculational model is presented for predicting ignition in coal dusts and particle suspensions. The P-3 spherical harmonics method is applied for the first time to predict radiative heat transfer in nongray planar and nonplanar enclosures with a range of particle sizes. This method has been extensively applied in neutron flux calculations in nuclear systems. The effect of the activation energy, optical thickness and the spectral properties of the particles on the temperature and the critical heat generation rates (Hc) are determined.

Ignition is observed to occur only when the activation energy is greater than a critical value which lies between 7 and 8. This is consistent with earlier investigations. It is found that the treatment of nongray media in terms of an equivalent gray model underestimates the temperature by upto about 12 percent in both planar and cylindrical enclosures, and to predict ignition at higher Hc values- by about 35 to 39 percent for both geometries.

CHAPTER I

INTRODUCTION

1.1 Overview

Fossil energy is being continuously depleted through various industrial and commercial applications and thus considerably affects the economy of any industrialized nation. Since natural resources such as coal and oil are non-replenishable, it is important to utilize these resources in an efficient manner and this necessitates an improved understanding of the combustion process/systems. There exists a great potential for improvement in the thermal performance of such systems; this could have a very positive effect on a country's economy and hence motivates research in combustion technology. Thus there is a need for developing computational models with optimal design of combustion systems so as to improve the performance of such systems.

Pulverized coal is finely crushed coal which can be burnt up very fast while in a state of suspension in air. It is used for producing high enthalpy steam which in turn is used to generate electricity. Combustion of pulverized coal is also used as a heat source for the manufacture of cement.

Combustion of pulverized coal is a difficult process to model mathematically; a complete and accurate model must take into consideration the treatment of three-dimensional two phase fluid dynamics, turbulent mixing, fuel evaporation, radiative and convective heat transfer and chemical kinetics. One would require comprehensive models incorporating all these factors in order to design combustion systems based on fundamental principles.

The role played by radiative transfer in coal combustion, pulverized coal fired boilers, industrial furnaces, gas turbine combustors and fires has been recogonized for some time. Radiation heat transfer plays a dominant role in most industrial furnaces and may account for up to 95% of the total heat transfer [1].

An adequate treatment of thermal radiation is essential in order to develop a mathematical model of pulverized coal combustion systems. The nature of the problem at hand - viz. whether one is interested in the instantaneous spectral local radiative flux, the flame structure, the scalar properties of the flame, formation of flame-generated particles (largely soot), the local radiative flux and its divergence or, the temperature distribution - would determine the complexity in the analytical treatment of the problem.

Combustion may be conceived of as a rapid and self accelerating oxidation of any given substance. We focus on combustion of pulverized coal particles in a combustion chamber. Heat is generated within the medium as a result of the exothermic oxidation of the coal particles. This is a source of photon production in the medium. The coal particles absorb, scatter and emit photons. The black walls surrounding the chamber also emit photons. Heat is removed from the system by being transferred to the boundaries.

Thermal equilibrium exists in the system when the heat production rate in the system is equal to the heat removal rate. It has been shown that two such equilibrium states are possible resulting from two possible temperature distributions in the medium [2, 3, 4]. The equilibrium corresponding to the higher temperature implies ignition of the coal

particles in the medium. It is desirable to be able to calculate the heat flux to the walls, the spatial temperature and intensity distribution in the system and the temperature at which the coal particles ignite, and to predict the dependence of these variables on the various physical and chemical characteristics of the medium; one would like to know the conditions which lead to the onset of ignition.

Radiation transfer from the flame and combustion products to the surrounding walls can be predicted if the radiative properties and the temperature distributions in the medium and the walls are known. In general, however, the temperature itself is an unknown variable, thus resulting in a coupling between the total energy and the radiant energy conservation equations.

A study of the equilibrium states, the determination of the temperature distribution and the heat flux variation in planar and cylindrical systems, and the dependence of these variables on the optical properties of the medium such as the optical thickness and the scattering albedo is the objective of the current thesis work.

1.2 Literature Survey

Gray and Lee [5] reviewed some of the earlier models in spontaneous ignition as applied to thermal explosion. In this review they have discussed the critical conditions obtained by the application of Semenov's model which assumes a uniform temperature distribution in the medium and Frank-Kamenetskii's theory which assumes a purely conductive heat transfer from the reacting medium to the surroundings, and have highlighted the limitations of these models.

Essenhigh and Csaba [6] analyzed the propagation of a plane flame

through a monodisperse dust cloud of finely ground coal in air. They solved three differential equations simultaneously :

(i) The equation describing the heat transfer by radiation from the flame to the dust,

(ii) The equation for the loss of heat by conduction from the particles to the ambient gas, and

(iii) The equation describing the rate of rise of the gas and particle temperatures.

With a series of simplifying assumptions, they obtained analytical solutions for the dust and gas temperatures, and the flame speed. They studied the behaviour of the flame speed with various parameters such as the input velocity of the dust, the ignition distance and time.

Arpaci and Tabaczynski [7] have investigated radiation effects in a laminar flame with combined modes of heat transfer involving both conduction and radiation; they have studied the effects of scattering, absorption and emission on the radiation flux as well as the variation in the thickness of the flame for varying conduction to radiation ratios.

Khalil et al [2] , studied ignition in a one-dimensional particle suspension system. They solved the following system of two simultaneous equations :

(i) The equation of transfer for the intensity (photon flux) variation,

(ii) The stationary energy balance between the radiative heat flux and the volumetric heat generation due to the chemical reactions in the combustion chamber as described by the diffusion limited Arrhenius equation.

Assuming elastic scattering, they studied the behavior of the

temperature distribution in response to the variation of particle size, scattering albedo and anisotropy in scattering. They also studied the variation in the maximum temperature in the system in response to the optical thickness of the suspension for various boundary conditions and compared the critical behavior for various boundary conditions. Mie theory [8], which approximates particles as spheres in order to solve the electromagnetic wave equations, was used for calculating the extinction and scattering efficiencies.

The study assumed a large initial positive value for the scattered and thermally emitted radiation in the suspension, the initial radiation thus serving as the ignition source. In a following study [9], two extreme cases of ignition in a particle suspension were investigated- one where the ignition was induced by an initial source as in the earlier study and the other where ignition was induced not by an initial thermal energy source but solely by thermal emission from the bounding walls. A comparative study was performed for the two cases.

Crosbie and Pattabongse [3] have compared several methods of calculating the temperature distribution for both uniform and Arrhenius heat generation in the medium and determined the critical heat generation for the two cases. They have studied the influence of the dimensionless activation energy α, the optical thickness τ_0 and the scattering albedo ω on the critical behavior; they found the value of the critical heat generation rate H_c to decrease with increasing τ_0 and increasing ω, and to increase with increasing α's. They also observed that increasing values of α brought about a more abrupt jump in the equilibrium state- thus causing increasingly intense ignition in the medium. The minimum

value of α required to cause ignition was determined to be around 7.5 for all cases.

In another investigation [10], they have studied transient heat transfer with both conduction and radiation in a planar medium. Again results have been presented for both uniform as well as Arrhenius heat generation in the medium. Besides the temperature distribution in the medium, parameters such as the time taken to reach steady state in regions close to the critical point, and the value of the critical point were studied in response to varying conduction/radiation ratios.

This brief review of past research in this field gives a flavor of the various developments in this area over the years; the recent works signify the current areas of interest and the nature of research being carried out presently.

1.3 Objectives

A mathematical model is developed to study thermal radiation in a pulverized coal suspension system. Although there is some precedence in this field [2, 3, 9 and 11], most of these studies have been limited to highly simplified models of the radiation processes taking place in a combustion chamber. These studies have been restricted to cases where all the particles are assumed to be of the same size, the radiation assumed to be monochromatic and the medium considered to be gray. All studies have been confined to plane geometry systems. The current thesis work is the first to treat in detail the combustion of pulverized coal particles in planar and cylindrical enclosures taking into account the wavelength dependence of the interaction coefficients of the the coal particles; such a medium is known as nongray and this wavelength

dependence is called the spectral behavior of the particles.

In practical situations there exists a distribution in the particle sizes. The bulk of particle diameters falls in the range 1μm to 100 μm. Such a distribution is often assumed to follow a mathematical law such as the Gaussian distribution for the number densities of the various particle diameters; it may also be chosen on the basis of a realistic sampling of various coal types, as is done in this study. The cross-sections of these particles are a function of the size (diameter) of the particle as well as the wavelength of the radiation. A very strong dependence on the wavelength leads to pronounced peaks in these cross-sections called "resonances". Such a dependence also results in a ripple structure in the cross-sections arising from the interference patterns. These resonances are reproduced in the corresponding interaction coefficients. Hence a monochromatic treatment of the radiation, with the cross-section assumed at the corresponding representative wavelength, could lead to significant inaccuracies in the results.

A more detailed model is developed in the current work to treat combustion in particle suspensions. The overall energy balance is assumed to involve two phenomena : (1) radiation transfer, and (2) internal heat generation in the system arising from the chemical kinetics of the reactions involved in combustion. The former is described by the equation of transfer and the latter by the Arrhenius heat generation equation; the required kinetic and diffusion parameters are assumed to be known *a priori*.

This study is limited to steady state conditions. Radiation is assumed

to be the sole mechanism of heat transfer. The model takes into account the wavelength dependence by treating radiation in a multigroup viz. discretized form. The CALLBH code [8] based on Mie theory [8] is modified to XSNGEN in order to generate the extinction and scattering cross-sections as a function of the particle size and wavelength. The cross-sections along with the particle size distribution, give the spectral extinction and scattering coefficients. These interaction coefficients are collapsed into a desired number of groups in order to discretize the wavelength variable λ; a FORTRAN code XSN.COLAPS is developed in order to do this. These coefficients then go into the equation of transfer for calculating the spatial distribution of the spectral intensity of radiation. The transfer equation and the energy equation are solved iteratively to determine the photon flux and temperature distributions in the system.

A computer code PN3 is written in FORTRAN 77 to solve the above equations in one dimensional planar and cylindrical geometries. The code is well structured and highly modular with further potential extensions easy to incorporate.

The code is applied to solve some representative numerical problems. Gray problems in planar geometry are first solved in order to compare the results with available results and validate the code. The effect of the non-dimensional activation energy α on ignition is compared for nongray and equivalent gray problems in planar geometry and the influence of the nongray effects is studied; this study is carried out for various optical thicknesses (τ).

One of the particle size distributions used by Menguc and Viskanta

[12] is considered for generating the cross-sections. A seven group structure in the wavelength range of 1μm - 30μm is assumed for the group interaction coefficients. Geometrical lengths of 0.1m and 0.2m are considered for the nongray models.

Finally, the above studies are repeated for cylindrical geometry in order to determine nongray effects in non-planar media.

CHAPTER II

THEORETICAL DEFINITION OF THE PROBLEM

2A: Radiative Transfer

Radiation is electromagnetic energy in transport. When radiant energy impinges on a particle, it results in a temporary excitation because of the increase in the energy level of the particle. As the particle returns to a lower energy level, it emits radiation in the form of one or more photons; it is called thermal radiation (detected in the form of heat and light) if the excitation comes by virtue of temperature.

Radiation is transmitted by electromagnetic waves in a wavelength range of 1 nm to 1 km, corresponding to X-rays and radiowaves respectively (Fig. 2-1). Thermal radiation falls in the range of 0.1-100 μm. This is the general range of interest in the treatment of combustion processes. However, the specific range in which the spectral dependence must be accounted for will largely depend on the variation in the cross-sections with wavelength and this range in the current study has been determined to be between 1 and 30 μm.

Owing to its dual nature, radiation may be treated either as waves or as particles. The particle nature leads to the application of Boltzmann's transport equation to solve for the photon density distribution in space viz. the spatial distribution of the spectral intensity of radiation.

2A.1 Equation of Transfer

Radiation traveling along a path is attenuated by absorption and by scattering into other directions, and is enhanced by both emission as

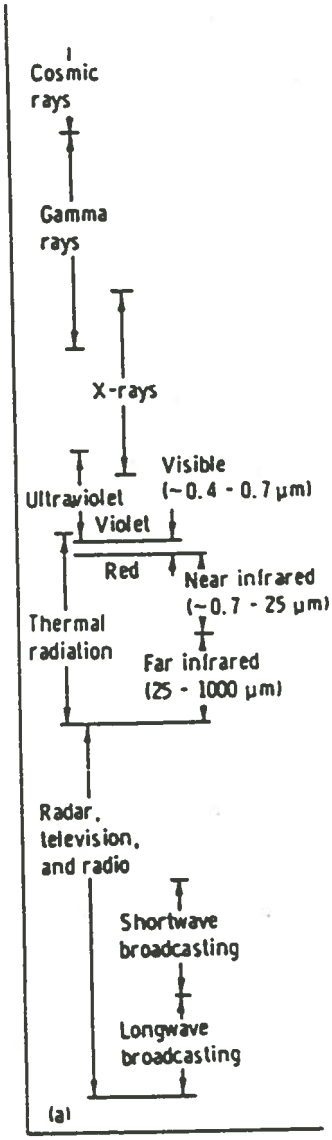

ELECTROMAGNETIC WAVE THEORY $c = \lambda\nu$

QUANTUM MECHANICS - Photons $E = h\nu$

THERMAL RADIATION - 0.1μ to 100μ

FIGURE 2-1

The Electromagnetic Spectrum (Ref. [13])

well as by radiation scattering in from other directions. The equation of transfer is a first order integro-differential equation which governs the radiation intensity along a path through a participating medium and undergoing absorption, emission and scattering.

Intensity is defined as the amount of radiation energy that is locally traveling in any given direction per unit solid angle and wavelength, and crossing a unit area normal to the direction of travel. The net energy crossing a unit area is obtained by integrating the product of the intensity and the direction vector, the integration being over all directions and wavelengths. This gives an equation for the local radiative heat flux, which when coupled with the energy balance equation in the system leads to a system of non-linear equations; the solution of this system of equations gives us

(i) The temperature distribution within the system, and

(ii) The radiation intensity distribution within the system.

The general steady state equation of transfer, assuming elastic scattering, for a 3-dimensional system of any geometry may be written as

$$\nabla.\hat{\Omega}\, i_\lambda(\hat{r},\hat{\Omega},\lambda) + \beta(\hat{r},\lambda)\, i_\lambda(\hat{r},\hat{\Omega},\lambda) = \kappa(\hat{r},\lambda)\, i_{b\lambda}(\hat{r},\lambda) + \int_{\hat{\Omega}'} \sigma_s(\hat{r},\hat{\Omega}'\to\hat{\Omega},\lambda)\, i_\lambda(\hat{r},\hat{\Omega}'\lambda)\, d\Omega' \qquad 2\text{-}1$$

where $\hat{r}$, $\hat{\Omega}$ and λ are the spatial, angular and wavelength variables respectively, $i_\lambda(\hat{r},\hat{\Omega},\lambda)$ is the spectral intensity, $i_{b\lambda}(\hat{r},\lambda)$ the blackbody intensity, and $\beta(\hat{r},\lambda)$, $\sigma_s(\hat{r},\hat{\Omega}'\to\hat{\Omega},\lambda)$ and $\kappa(\hat{r},\lambda)$ are the extinction, scattering and absorption coefficients respectively.

For a homogeneous medium, there is no spatial dependence of the

interaction coefficients and only their spectral variation needs to be considered. In theory, the variation of the interaction coefficients with wavelength must be treated as a continuous function; this however is not very practical because of the complex functions which describe the spectral behavior of the interaction coefficients based on the electromagnetic theory of radiation. Instead, the wavelength can be discretized into a finite number of intervals called wavelength 'groups' (a term often used in neutronics calculations to refer to the energy variable) and all quantities integrated over these groups to arrive at an average or representative value for each group. Such a formulation is known as the multi-group method, and results in the multi-group equations.

2A.2 Multigroup transfer equation

Defining a group 'g' between the wavelength limits λ_{gl} and λ_{gu} and integrating equation 2-1 over 'g'

$$\nabla.\hat{\Omega} \int_{\lambda_{gl}}^{\lambda_{gu}} i_\lambda(\hat{r},\hat{\Omega},\lambda)\, d\lambda + \int_{\lambda_{gl}}^{\lambda_{gu}} \beta(\lambda)\, i_\lambda(\hat{r},\hat{\Omega},\lambda)\, d\lambda$$
$$= \int_{\lambda_{gl}}^{\lambda_{gu}} \kappa(\lambda)\, i_{b\lambda}(\hat{r},\lambda)\, d\lambda + (1/4\pi)\int_{\hat{\Omega}'} \left[\int_{\lambda_{gl}}^{\lambda_{gu}} \sigma_s(\lambda)\, i_\lambda(\hat{r},\hat{\Omega}',\lambda)\, d\lambda \right] d\Omega' \qquad 2\text{-}2$$

with the assumption that scattering is elastic and isotropic [2].

These groups are defined so that the interaction coefficients are averaged within each group and the intensity is integrated over the group; the following group quantities are defined

$$i_g(\hat{r},\hat{\Omega}) = \int_{\lambda_{gl}}^{\lambda_{gu}} i_\lambda(\hat{r},\hat{\Omega},\lambda)\, d\lambda = \text{intensity for group 'g',}$$

$$i_{bg}(\hat{r}) = \int_{\lambda_{gl}}^{\lambda_{gu}} i_{b\lambda}(\hat{r},\lambda)\, d\lambda \quad = \text{black body intensity for group 'g'}$$

and β_g, κ_g, and σ_{sg}, are respectively the extinction, absorption and the scattering coefficients for group 'g'. These coefficients are given as

$$\gamma_g = \frac{\int_{\lambda_{gl}}^{\lambda_{gu}} \gamma(\lambda) i_\lambda(\hat{r},\hat{\Omega},\lambda)\, d\lambda}{\int_{\lambda_{gl}}^{\lambda_{gu}} i_\lambda(\hat{r},\hat{\Omega},\lambda)\, d\lambda}$$

where γ_g represents β_g, κ_g or σ_{sg}. In practice, since the intensity distribution is not known beforehand, other functions such as the Planck and Rosseland weighting functions which are assumed to represent the intensity variation, are used to determine the interaction coefficients. These are discussed in section 3.3.

Incorporating the above definitions in equation 2-2, we get

$$\nabla.\hat{\Omega}\, i_g(\hat{r},\hat{\Omega}) + \beta_g i_g(\hat{r},\hat{\Omega}) = \kappa_g i_{bg}(\hat{r}) + (\sigma_{sg}/4\pi)\int_{\hat{\Omega}'} i_g(\hat{r},\hat{\Omega}')\, d\Omega' \qquad 2\text{-}3$$

Equation 2-3 is the general three-dimensional multigroup form of the equation of transfer for any geometry.

2A.3 Spectral and group radiative heat flux

Integrating equation 2-1 over all directions ($\hat{\Omega} = 0\text{-}4\pi$)

$$\nabla.\int_{\hat{\Omega}} \hat{\Omega}\, i_\lambda(\hat{r},\hat{\Omega},\lambda)\, d\Omega + \beta(\hat{r},\lambda)\int_{\hat{\Omega}} i_\lambda(\hat{r},\hat{\Omega},\lambda)\, d\Omega = \kappa_\lambda(\hat{r},\lambda)\, i_{b\lambda}(\hat{r},\lambda)\int_{\hat{\Omega}} d\Omega$$
$$+ [\sigma_s(\hat{r},\lambda)/4\pi]\int_{\hat{\Omega}} \left[\int_{\hat{\Omega}'} i_\lambda(\hat{r},\hat{\Omega}',\lambda)\, d\Omega' \right] d\Omega \qquad 2\text{-}4$$

From the definition of the radiative heat flux ($\vec{q}''_R$) and the scalar flux (i_0)

$$\nabla.\vec{q}''_{R\lambda}(\hat{r},\lambda) + \beta(\hat{r},\lambda)\ i_{0\lambda}(\hat{r},\lambda) = 4\pi\ \kappa(\hat{r},\lambda)\ i_{b\lambda}(\hat{r},\lambda) + \sigma_s(\hat{r},\lambda)\ i_{0\lambda}(\hat{r},\lambda) \qquad 2\text{-}5$$

Rearranging the terms and noting that

$$\sigma_s(\hat{r},\lambda) - \beta(\hat{r},\lambda) = -\kappa(\hat{r},\lambda) \qquad \text{we get}$$

$$\nabla.\vec{q}''_{R\lambda}(\hat{r},\lambda) = \kappa(\hat{r},\lambda)\left[\ 4\pi i_{b\lambda}(\hat{r},\lambda) - i_{0\lambda}(\hat{r},\lambda)\ \right] \qquad 2\text{-}6$$

The above equation describes the spectral radiative heat flux vector $\vec{q}''_{R\lambda}(\hat{r},\lambda)$.

Integrating equation 2-6 over 'g' for a homogeneous medium and recalling the earlier definitions, we can write

$$\nabla.\int_{\lambda_{gl}}^{\lambda_{gu}} \vec{q}''_{R\lambda}(\hat{r},\lambda)\ d\lambda = \int_{\lambda_{gl}}^{\lambda_{gu}} \kappa(\hat{r},\lambda)\left[4\pi i_{b\lambda}(\hat{r},\lambda) - i_{0\lambda}(\hat{r},\lambda)\right] d\lambda \qquad 2\text{-}7$$

Define

$$\int_{\lambda_{gl}}^{\lambda_{gu}} i_{0\lambda}(\hat{r},\lambda)\ d\lambda = i_{0g}(\hat{r}) = \text{scalar flux for group 'g'}$$

$$\int_{\lambda_{g\lambda}}^{\lambda_{gu}} \vec{q}''_{R\lambda}(\hat{r},\lambda)\ d\lambda = \vec{q}''_{Rg}(\hat{r}) = \text{radiative heat flux for group 'g'}$$

Hence

$$\nabla.\vec{q}''_{Rg}(\hat{r}) = \kappa_g\left[4\pi i_{bg}(\hat{r}) - i_{0g}(\hat{r})\right] \qquad 2\text{-}8$$

Summing over all the groups (g =1, NG) which represent the entire wavelength range $0 < \lambda < \infty$

$$\nabla . \sum_{g=1}^{NG} \vec{q}''_{Rg}(\hat{r}) = \nabla . \vec{q}''_{R}(\hat{r}) = \sum_{g=1}^{NG} \kappa_g \left[4\pi i_{bg}(\hat{r}) - i_{0g}(\hat{r}) \right] \qquad 2\text{-}9$$

where $\vec{q}''_{R}(\hat{r})$ is the total radiative heat flux.

2A.4 Solution of Multigroup Equations

The above set of equations can be solved for the radiation intensity and the radiative heat flux in each group if the temperature distribution in the medium is given; this would give expressions for the emitted radiation, and equation 2-3 can be solved for $i_{0g}(\hat{r})$. This can be inserted in equation 2-9 to solve for the radiative heat flux.

Over the last few decades, many analytical and numerical methods have evolved for solving the transfer equation. Since analytical solutions are not possible except for a few idealized cases, numerical schemes are generally resorted to. These schemes involve discretization of the space, wavelength and angular variables.

The Hottel's zone method involves subdividing the system into a set of volume and surface zones with uniform properties, and applying the energy balance to each zone. However, a large number of zones are required to obtain accurate solutions, thus increasing the computation costs. The diffusion approximation is applicable when the medium is optically thick and the absorption to extinction ratio is low, and results in a differential equation that resembles the heat conduction equation which can be solved using finite difference numerical schemes. The Monte Carlo method is a statistical simulation scheme and has been

used to study radiative transfer in concentric and full cylinders and radiative heat flux in cylindrical furnaces. However, a good number of 'histories' have to be considered in order to obtain accurate results.

The discrete ordinates method has been widely used in recent years; it involves dividing the total direction domain into discrete directions and solving for the radiation intensity in each direction. But the solutions tend to become expensive in a problem such as ours where it is necessary to solve iteratively for the scalar flux and the temperature distribution.

The P_N method has been found to give accurate results over a broad range of optical thicknesses [14, 15, 16]. It has been widely applied in many nuclear engineering problems for neutron flux calculations. Equations known as moment equations can be obtained by successively multiplying the transfer equation by powers of the direction cosine and integrating over all directions. The direction cosine is μ (= $\text{Cos}\theta$) in the planar geometry (Fig. 2-2) and l_r (= $\text{Sin}\theta.\text{Cos}\varphi$) in cylindrical geometry (Fig. 2-3). These can then be cast into a matrix form and solved directly using the matrix solving routines in IMSL (International Math and Statistical library) available in the IBM mainframe computer. Hence this method has been adopted in this study.

The P_N method is based on Spherical Harmonic functions which are discussed briefly in the following section.

2A.5 Spherical Harmonics

The Spherical harmonics method employed in the development of the code for this study is exact in its broadest sense. Spherical harmonics are a set of mathematical functions in the angular variables μ (= $\cos\theta$)

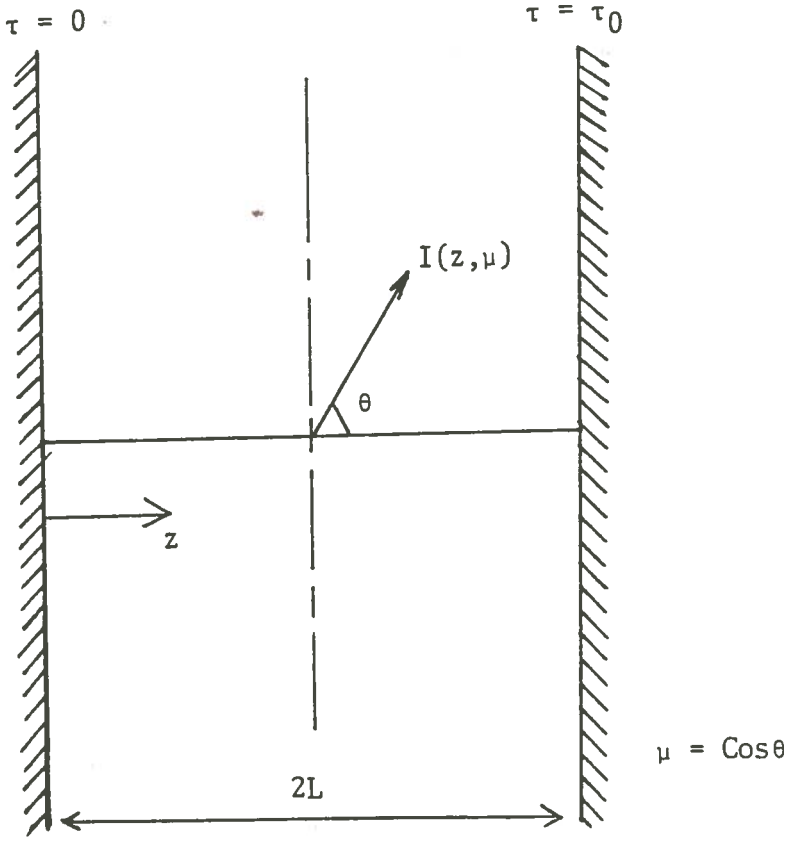

FIGURE 2-2

Coordinate System Showing Intensity as a Function of Position and Angle for a Slab Geometry

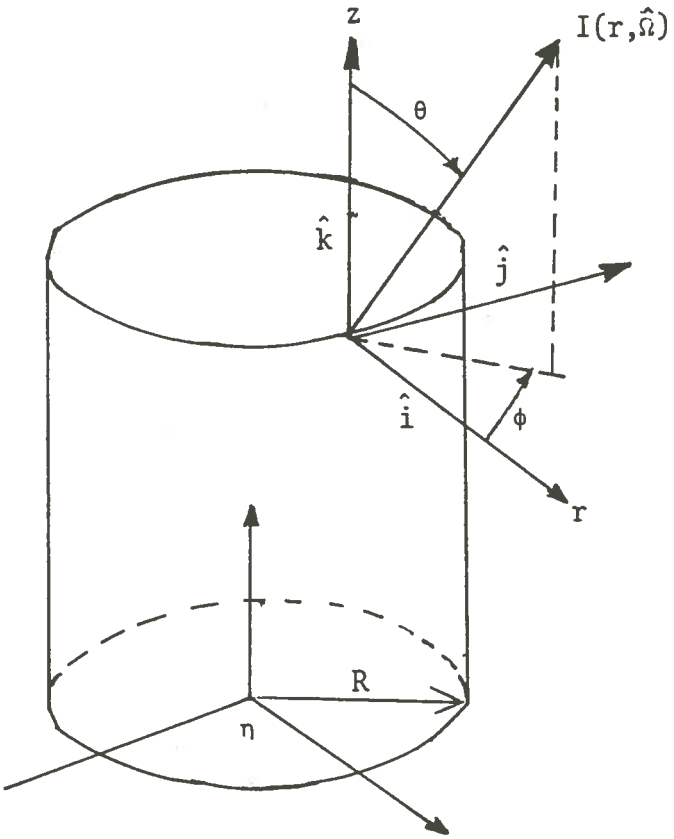

$l_z = \cos\theta$

$l_r = \sin\theta \cos\phi$

$l_\eta = \cos\theta \cos\phi$

FIGURE 2-3

Coordinate System Showing Intensity as a Function of Position and Angle for a Cylindrical Geometry

and φ that determine the direction vector $\hat{\Omega}$. They are defined as

$$Y_n^m(\hat{\Omega}) = Y_n^m(\mu,\varphi) = \left\{ \frac{(2n + 1)(n - m)!}{(n + m)!} \right\}^{1/2} P_n^m(\mu)\exp(im\varphi)$$

where n is a positive integer or zero, $-n \leq m \leq n$, and $P_n^m(\mu)$ are the associated Legendre polynomials defined as

$$P_n^m(\mu) \equiv (1 - \mu^2)^{m/2} \frac{d^m}{d\mu^m} P_n(\mu), \qquad \text{and}$$

$$P_n^{-m}(\mu) \equiv (-1)^m \frac{(n - m)!}{(n + m)!} P_n^m(\mu)$$

$P_n(\mu)$ in turn are the Legendre polynomials defined such that

$$P_0(\mu) = 1$$

$$P_1(\mu) = \mu$$

$P_n(\mu)$ for any other $n > 1$ can be detemined using the recursion relationship

$$(2n + 1)\mu P_n(\mu) = (n+1)P_{n+1}(\mu) + nP_{n-1}(\mu)$$

For one-dimensional planar geometry 'm' is always zero and the spectral intensity can be expanded as an orthogonal series of the Legendre polynomials to give

$$i_\lambda(z,\mu,\lambda) = \sum_{n=0}^{\infty} \frac{2n+1}{4\pi} P_n(\mu)A_n(z,\lambda)$$

where the coefficients A_n can be written in terms of the intensity moments. The first three P_n and A_n (for a P_3 approximation) are given as

$$P_0 = 1 \qquad A_0 = i_{0\lambda}(z,\lambda)$$

$$P_1 = \mu \qquad A_1 = i_{1\lambda}(z,\lambda)$$

$$p_2 = (1/2)(3\mu^2-1) \qquad A_2 = (1/2)[3i_{2\lambda}(z,\lambda) - i_{0\lambda}(z,\lambda)]$$

$$p_3 = (1/2)\mu(5\mu^2-3) \qquad A_3 = (1/2)[5i_{3\lambda}(z,\lambda) - 3i_{1\lambda}(z,\lambda)]$$

where i_0, i_1 and i_2 are the intensity moments given by

$$i_{n\lambda}(z,\lambda) = \int_{4\pi} \mu^n \, i_\lambda(z,\mu,\lambda) \, d\Omega$$

For one-dimensional cylindrical geometry under azimuthal symmetry, the intensity distribution becomes an even function of φ and may be expanded as [15]

$$i_\lambda(r,\mu,\varphi,\lambda) = \sum_{n=0}^{\infty} \sum_{m=0}^{n} \frac{2n+1}{8\pi} [1 + (-1)^{n+m}] \, P_n^m(\mu) \left[A_n^m(r,\lambda)\cos(m\varphi)\right]$$

The associated Legendre polynomials P_n^m and the coefficients A_n^m for the cylindrical geometry are discussed in reference [15].

Thus far no approximation has been introduced; if the series were fully represented by an infinite series i.e. 'n' allowed to take on values from zero to infinity, then the treatment is exact. In practice, the series is truncated after a finite number (N) of terms; this leads to what are known as the P_N approximations. The number of terms considered depends on the physical nature of the problem. For isotropic variations in intensity P_1 or P_3 expansions are normally used. For anisotropic problems it may be necessary to resort to higher order approximations. Higenyi [15] has obtained solutions using P_3 and P_5 approximations. This method has also been applied by Yucel and Bayazitoglu to investigate radiative transfer in nongray planar media [14]. The current study

considers the P_3 approximation.

2A.6 Moment equations and boundary conditions

2A.6.1 One dimensional Planar Geometry

Substituting the expressions for the coefficients A_n and the Legendre polynomials $P_n(\mu)$, the spectral intensity $i_\lambda(z,\mu,\lambda)$ for a one-dimensional planar geometry may be expanded in a P_3 approximation to give

$$i_\lambda(z,\mu,\lambda) = (1/4\pi)\Big[\, i_{0\lambda}(z,\lambda) + 3\mu i_{1\lambda}(z,\lambda) + (5/4)(3\mu^2-1)[3i_{2\lambda}(z,\lambda) - i_{0\lambda}(z,\lambda)] + (7/4)(5\mu^3-3\mu)[5i_{3\lambda}(z,\lambda) - 3i_{1\lambda}(z,\lambda)] \,\Big] \qquad 2\text{-}10$$

Integrating over λ, this may be cast in the multigroup form as

$$i_g(z,\mu) = (1/4\pi)\Big[\, i_{0g}(z) + 3\mu i_{1g}(z) + (5/4)(3\mu^2-1)[3i_{2g}(z) - i_{0g}(z)] + (7/4)(5\mu^3-3\mu)[5i_{3g}(z) - 3i_{1g}(z)] \,\Big] \qquad 2\text{-}11$$

The multigroup transfer equation for the intensity of radiation in a homogeneous medium (with constant interaction coefficients over space) may be written as

$$\mu \frac{\delta i_g(z,\mu)}{\delta z} = \kappa_g\, i_{bg}(z) - \beta_g\, i_g(z,\mu) + \frac{\sigma_{sg}}{4\pi} \int_{4\pi} i_g'(z,\mu')\, d\Omega' \qquad 2\text{-}12$$

Noting that the integral in the last term of the above equation is the scalar flux $i_{0g}(z)$, the above equation may be rewritten as

$$\mu \frac{di_g(z,\mu)}{dz} = \kappa_g\, i_{bg}(z) - \beta_g\, i_g(z,\mu) + \left(\frac{\sigma_{sg}}{4\pi}\right) i_{0g}(z) \qquad 2\text{-}13$$

As mentioned in the previous section, the above equation is successively multiplied by $\mu^{(k)}$ for k = 0, 1, 2, 3 (and equation 2-11 substituted for $i_g(z,\mu)$) and then integrated to yield the following

moment equations

$$\frac{di_{1g}(z)}{dz} = \kappa_g(4e_{bg}(z) - i_{0g}(z)) \qquad 2\text{-}14(a)$$

$$\frac{di_{2g}(z)}{dz} = -(\kappa_g + \sigma_{sg})\, i_{1g}(z) = -\beta_g\, i_{1g}(z) \qquad 2\text{-}14(b)$$

$$\frac{di_{3g}(z)}{dz} = (4/3)\,\kappa_g e_{bg}(z) - \beta_g\, i_{2g}(z) + (\sigma_{sg}/3)\, i_{0g}(z) \qquad 2\text{-}14(c)$$

$$\frac{di_{4g}(z)}{dz} = -\beta_g i_{3g}(z) \qquad 2\text{-}14(d)$$

and the closure condition

$$i_{4g}(z) = (6/7)i_{2g}(z) - (3/35)i_{0g}(z) \qquad 2\text{-}15$$

where $e_{bg}(z)$ is the hemispherical emissive power for group 'g' and is given by

$$e_{bg}(z) = \pi i_{bg}(z) = 4F_g\hat{\sigma}T^4(z)$$

where $F_g = F_{0-\lambda l} - F_{0-\lambda u}$ is the black body fraction [13] for group 'g', $\hat{\sigma}$ is the Stefan-Boltzmann constant, and T(z) is the temperature at z.

We define the following normalized quantities

$$\tau = \beta_m\, z \;;\quad d\tau = \beta_m\, dz \;;\quad D[\ ] = d/d\tau[\ ]$$

$$\omega_g = \sigma_{sg}/\beta_g \;;\quad \alpha_g = \beta_g/\beta_m$$

$$I_{kg}(z) = i_{kg}(z)/4\hat{\sigma}T_r^4 \;;\qquad \Theta(z) = T(z)/T_r$$

$$E_{bg}(z) = e_{bg}(z)/\hat{\sigma}T_r^4 = 4F_g\Theta^4(z)$$

where β_m is the maximum extinction coefficient, τ represents the optical

length, ω_g is the scattering albedo for group 'g', α_g is the ratio of the extinction coefficient for group 'g' to β_m, T_r is the reference temperature and $i_{kg}(z)$ represents the k'th moment for group 'g'.

Dividing the equations 2-14 and 2-15 all through by $4\beta_m\hat{\sigma}T_r^4$ the moment equations may be rewritten in terms of the normalized quantities

$$DI_{1g}[\tau] = \alpha_g(1-\omega_g)[E_{bg}(\tau) - I_{0g}(\tau)] \qquad 2\text{-}16(a)$$

$$DI_{2g}[\tau] = -\alpha_g I_{1g}(\tau) \qquad 2\text{-}16(b)$$

$$DI_{3g}[\tau] = \alpha_g[(1-\omega_g)/3]\, E_{bg}(\tau) - \alpha_g I_{2g}(\tau) + (\alpha_g\omega_g/3)\, I_{0g}(\tau) \qquad 2\text{-}16(c)$$

$$DI_4[\tau] = -\alpha_g I_{3g}(\tau) \qquad 2\text{-}16(d)$$

and

$$I_{4g}(\tau) = (6/7)\, I_{2g}(\tau) - (3/35)\, I_{0g}(\tau) \qquad 2\text{-}17$$

The above set of four linear differential equations are manipulated arithmetically to give the following set of two second order differential equations

$$D^2I_{0g}[\tau] + \alpha_g^2\left[(35/3)I_{2g}(\tau) - \left\{10(1-\omega_g) + (35/9)\omega_g\right\} I_{0g}(\tau) + (55/9)(1-\omega_g)\, E_{bg}(\tau)\right] = 0 \qquad 2\text{-}18(a)$$

$$D^2I_{2g}[\tau] + \alpha_g^2(1-\omega_g)[E_{bg}(\tau) - I_{0g}(\tau)] = 0 \qquad 2\text{-}18(b)$$

Boundary conditions

Marshak boundary conditions [15] are applied to the two boundaries which are assumed to be black walls maintained at constant temperatures T_1 (at z = 0) and T_2 (at z = 2L) respectively. Thus

$$\int_{\mu=0}^{-1} \mu^{(k)}\, i_g(z,\mu)\, d\Omega = \int_{\mu=0}^{-1} \mu^{(k)}\, i_{bg}(z)\, d\Omega \qquad k = 1,\ 3,\ 5\ldots \qquad 2\text{-}19(a)$$

$$\int_{\mu=-1}^{0} \mu^{(k)}\, i_g(z,\mu)\, d\Omega = \int_{\mu=-1}^{0} \mu^{(k)}\, i_{bg}(z)\, d\Omega \qquad k = 1,\ 3,\ 5\ldots \qquad 2\text{-}19(b)$$

for $z = 0$ and $z = 2L$ respectively.

Substituting equation 2-11 for $i_g(z,\mu)$ in equation 2-19 and evaluating the integrals for $k = 1$ and $k = 3$ we get

at $\underline{z = 0}$ $(\tau = 0)$

$$3i_{0g}(0) - 16i_{1g}(0) + 15i_{2g}(0) = 32e_{bg}(0) \qquad 2\text{-}20(a)$$

$$-2i_{0g}(0) + 30i_{2g}(0) - 32i_{3g}(0) = 32e_{bg}(0) \qquad 2\text{-}20(b)$$

and at $\underline{z = 2L}$ $(\tau = \tau_0)$

$$3i_{0g}(\tau_0) + 16i_{1g}(\tau_0) + 15i_{2g}(\tau_0) = 32e_{bg}(\tau_0) \qquad 2\text{-}21(a)$$

$$-2i_{0g}(\tau_0) + 30i_{2g}(\tau_0) + 32i_{3g}(\tau_0) = 32e_{bg}(\tau_0) \qquad 2\text{-}21(b)$$

Dividing through by the factor $4\hat{\sigma}T_r^4$ the above equations may be written in terms of the normalized quantities as

$$3I_{0g}(0) - 16I_{1g}(0) + 15I_{2g}(0) = 8E_{bg}(0) \qquad 2\text{-}22(a)$$

$$-2I_{0g}(0) + 30I_{2g}(0) - 32I_{3g}(0) = 8E_{bg}(0) \qquad 2\text{-}22(b)$$

$$3I_{0g}(\tau_0) + 16I_{1g}(\tau_0) + 15I_{2g}(\tau_0) = 8E_{bg}(\tau_0) \qquad 2\text{-}23(a)$$

$$-2I_{0g}(\tau_0) + 30I_{2g}(\tau_0) + 32I_{3g}(\tau_0) = 8E_{bg}(\tau_0) \qquad 2\text{-}23(b)$$

Eliminating I_{1g} and I_{3g} using the moment equations 2-16

$\underline{\tau = 0}$

$$3\,\alpha_g I_{0g}(0) + 15\,\alpha_g I_{2g}(0) - 16\,DI_{2g}[0] - 8\,\alpha_g F_g \theta_1^4 = 0 \qquad 2\text{-}24(a)$$

$$-2\,\alpha_g I_{0g}(0) + 30\,\alpha_g I_{2g}(0) - (192/7)DI_{2g}[0] + (96/35)DI_{0g}[0] - 8\,\alpha_g F_g \theta_1^4 = 0 \qquad 2\text{-}24(b)$$

$\underline{\tau = \tau_0}$

$$3\,\alpha_g I_{0g}(\tau_0) + 15\,\alpha_g I_{2g}(\tau_0) + 16\,DI_{2g}[\tau_0] - 8\,\alpha_g F_g \theta_2^4 = 0 \qquad 2\text{-}25(a)$$

$$-2\,\alpha_g I_{0g}(\tau_0) + 30\,\alpha_g I_{2g}(\tau_0) + (192/7)DI_{2g}[\tau_0] - (96/35)DI_{0g}[\tau_0] - 8\,\alpha_g F_g \theta_2^4 = 0 \qquad 2\text{-}25(b)$$

2A.6.2 <u>One dimensional Cylindrical Geometry</u>

The multigroup transfer equation for this case may be written as

$$l_r \frac{di_g(r,\theta,\varphi)}{dr} - (1/r) l_\eta \frac{di_g(r,\theta,\varphi)}{d\varphi} = -\beta_g i_g(r,\theta,\varphi) + \kappa_g i_{bg}(r) + (\sigma_g/4\pi) i_{0g}(r) \qquad 2\text{-}26$$

where l_r and l_η are the direction cosines along the r and η directions and are given (from figure 2-3) as

$$l_r = \sin(\theta).\cos(\varphi) \; ; \quad l_\eta = \cos(\theta).\cos(\varphi)$$

Multiplying the above equation successively by powers of l_r ($l_r^{(k)}$ for k = 0, 1, 2, 3) the following moment equations may be derived for the P_3 approximation [15]

$$(1/r) \frac{d}{dr}\left[r i_{1g}(r)\right] = \kappa_g [4 e_{bg}(r) - i_{0g}(r)] \qquad 2\text{-}27(a)$$

$$(1/r^2)\frac{d}{dr}\left[r^2 i_{2g}(r)\right] = -\beta_g i_{1g}(r) + (\frac{2}{3r})i_{0g}(r) \qquad 2\text{-}27(b)$$

$$(1/r^3)\frac{d}{dr}\left[r^3 i_{3g}(r)\right] = -\beta_g i_{2g}(r) + (\frac{8}{5r})i_{1g}(r) + (\sigma_{sg}/3)i_{0g}(r) + (4\kappa_g/3)e_{bg}(r) \qquad 2\text{-}27(c)$$

$$(1/r^4)\frac{d}{dr}\left[r^4 i_{4g}(r)\right] = -\beta_g i_{3g}(r) + (18/7)i_{2g} - (\frac{2}{35r})i_{0g}(r) \qquad 2\text{-}27(d)$$

and the closure condition

$$i_{4g}(r) = (6/7)i_{2g}(r) - (3/35)i_{0g}(r) \qquad 2\text{-}28$$

Defining the following normalized quantities

$$\tau = \beta_m r \; ; \quad d\tau = \beta_m dr \; ; \quad D[\;] = d/d\tau[\;]$$

and recalling the earlier definitions, the above equations may be rewritten in terms of the normalized quantities as

$$(1/\tau)D[\tau I_{1g}(\tau)] = \alpha_g(1-\omega_g)[E_{bg}(\tau) - I_{0g}(\tau)] \qquad 2\text{-}29(a)$$

$$(1/\tau^2)D[\tau^2 I_{2g}(\tau)] = -\alpha_g I_{1g}(\tau) + (\frac{2}{3\tau})I_{0g}(\tau) \qquad 2\text{-}29(b)$$

$$(1/\tau^3)D[\tau^3 I_{3g}(\tau)] = -\alpha_g I_{2g}(\tau) + (\frac{8}{5\tau})I_{1g}(\tau) + (\alpha_g\omega_g/3)I_{0g}(\tau) + \alpha_g[(1-\omega_g)/3]\,E_{bg}(\tau) \qquad 2\text{-}29(c)$$

$$(1/\tau^4)D[\tau^4 I_{4g}(\tau)] = -\alpha_g I_{3g}(\tau) + (\frac{18}{7\tau})I_{2g}(\tau) - (\frac{2}{35\tau})I_{0g}(\tau) \qquad 2\text{-}29(d)$$

and

$$I_{4g}(\tau) = (6/7)I_{2g}(\tau) - (3/35)I_{0g}(\tau) \qquad 2\text{-}30$$

Again the above set of four linear differential equations may be reduced to the following set of two second order differential equations

$$D^2 I_{0g}[\tau] - (\frac{1}{3\tau})DI_{0g}[\tau] + (\frac{26}{3\tau})DI_{2g}[\tau] + \alpha_g^2\Big[\Big\{\Big(\frac{52}{3\tau^2}\Big) + (35/3)\Big\}I_{2g}(\tau) - \Big\{\Big(\frac{52}{9\tau^2}\Big) + 10(1-\omega_g) + [(35/9)\omega_g]\Big\}I_{0g}(\tau) + (55/9)(1-\omega_g)E_{bg}(\tau)\Big] = 0 \qquad 2\text{-}31(a)$$

$$D^2 I_{2g}[\tau] + (\frac{3}{\tau})DI_{2g}[\tau] - (\frac{2}{3\tau})DI_{0g}[\tau] + \alpha_g^2(1-\omega_g)[E_{bg}(\tau) - I_{0g}(\tau)] = 0 \qquad 2\text{-}31(b)$$

Boundary conditions :

The Marshak boundary condition [15] is applied at the surface of the cylinder ($\tau = \tau_0$) which is assumed to be a black wall maintained at a constant temperature T_2; a reflected boundary condition is applied at the center of the cylinder where the temperature, the scalar flux and the spectral radiative heat flux are maximum. Hence we get the following set of boundary conditions

$\tau = 0$

$$DI_{0g}(0) = 0 \qquad 2\text{-}32(a)$$

$$DI_{2g}(0) = 0 \qquad 2\text{-}32(b)$$

$\tau = \tau_0$

$$3(\alpha_g - \frac{32}{3\tau_0})I_{0g}(\tau_0) + (15\alpha_g + \frac{32}{\tau_0})I_{2g}(\tau_0) + 16DI_{2g}[\tau_0] - 8\alpha_g F_g \theta_2^4(\tau_0) = 0 \qquad 2\text{-}33(a)$$

$$-(2\alpha_g + \frac{64}{7\tau_0})I_{0g} + (30\alpha_g + \frac{192}{7\tau_0})I_{2g}(\tau_0) + (\frac{192}{7})DI_{2g}[\tau_0] - (\frac{96}{35})DI_{0g}[\tau_0] - 8\alpha_g F_g \theta_2^4(\tau_0) = 0 \qquad 2\text{-}33(b)$$

2B: Thermal Equilibrium and Ignition

2B.1 Heat generation

This study concerns radiative heat transfer in a medium with heat generation which is temperature dependent. This heat generation results from the exothermic nature of the oxidation reaction of pulverized coal and can be described by the Arrhenius equation [2]

$$H(\hat{r}) = A \, Exp[-E/RT(\hat{r})] \qquad 2\text{-}34$$

where R is the universal gas constant.

The quantity E is called the activation energy for the reaction and depends on the chemical kinetics of the reaction; 'A' is known as the pre-exponential factor and depends on the physical conditions, such as the temperature and pressure, existing in the medium.

Normalizing the temperature $T(\hat{r})$ and the activation energy E with respect to the reference temperature T_r, we define

$$\theta(\hat{r}) = T(\hat{r})/T_r$$

$$\alpha = E/RT_r$$

Hence the above equations may be rewritten in terms of the normalized quantities as

$$H(\hat{r}) = A \, Exp[-\alpha/\theta(\hat{r})] \qquad 2\text{-}35$$

Rewriting the above equation in terms of the optical length τ

$$H(\tau) = A \, Exp[-\alpha/\theta(\tau)] \qquad 2\text{-}36$$

2B.2 Overall energy balance

Neglecting conductive and convective heat transfer, the net energy

balance for a differential volume ΔV may be written as

Heat generated in ΔV = heat radiated from ΔV

Thus

$$H(\tau).\Delta V = \nabla.\vec{q}_R^{\,w}(\tau).\Delta V$$

Substituting equations 2.9 and 2.36 and recalling all the previous normalizations

$$A\ Exp[-\alpha/\theta(\tau)] = \sum_{g=1}^{IGM} \alpha_g(1-\omega_g)[E_{bg}(\tau) - I_{0g}(\tau)] \qquad 2\text{-}37$$

2B.3 Thermal Equilibrium

The theory of combustion deals with the combined system of equations of chemical kinetics, heat transfer and diffusion. The reaction rate always depends on the temperature in a non-linear fashion (given by the Arrehenius expression). Such a non-linearity is an important characteristic of combustion phenomena.

Thermodynamic equilibrium is achieved only if there is sufficient time for all the reactions to reach their equilibrium state. In the burning of coal, such a state is referred to as "thermal equilibrium" viz. an equilibrium between the rate of heat generation from the chemical reactions involved and the rate of heat removal from the system by radiative transfer. The study of such equilibrium states helps in predicting the onset of ignition in the coal particles.

Ignition results from a non-feasibility of equilibrium between the reacting system and the surrounding medium. This depends on the parameters affecting the reaction rate and the release of heat or active

products into the medium. Ignition can be brought about by changing any of the following parameters

(i) The physical properties of the mixture such as the temperature, pressure, composition, coefficient of thermal diffusivity and the diffusion coefficient.

(ii) The dimensions of the system.

Ignition may also be brought about by an artificially induced disturbance to the equlibrium state which exists for the given initial conditions.

Figure 2-4 gives a typical heat generation rate variation in a combustion chamber. The coal suspension is assumed to be maintained at a temperature T. With all the other parameters such as fuel type, particle size and the fuel/air flow rate invariant, the figure illustrates the dependence of the volumetric heat generation rate H on the temperature T at that location in the medium. It is observed that H starts off at a low value for low temperatures, rises steeply with increasing temperatures, and finally levels off at a value H_0 (which depicts the maximum value for that fuel supply and the onset of diffusion control in the reaction). For an efficient production of energy it is desirable to design the combustion chamber such that H approaches H_0 at as high a temperature as possible.

Figure 2-5 illustrates a typical heat removal rate Q_R ($= \nabla . q_R''$ (0)) curve for fixed wall temperature T_w; the curve shows the dependence of this function on T_w.

Superposition of figures 2-4 and 2-5, viz. the rate of heat generation and heat loss, gives the equilibrium states in the system.

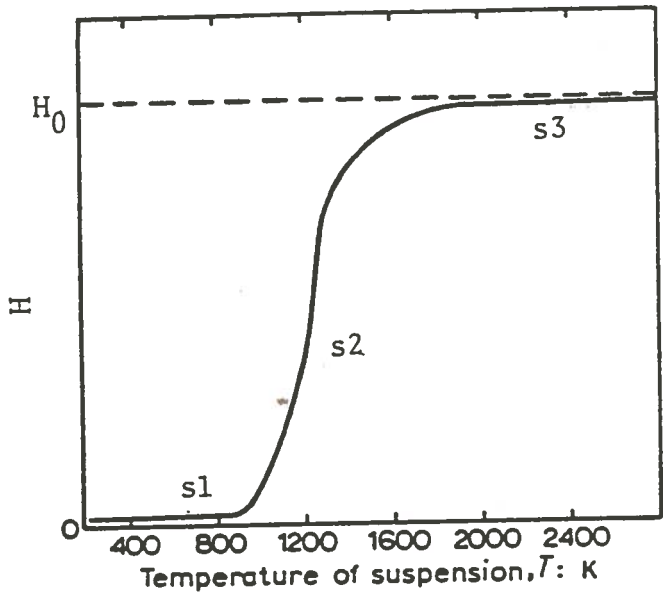

FIGURE 2-4

Heat Generation Rate as a Function of Temperature (Ref. [4])

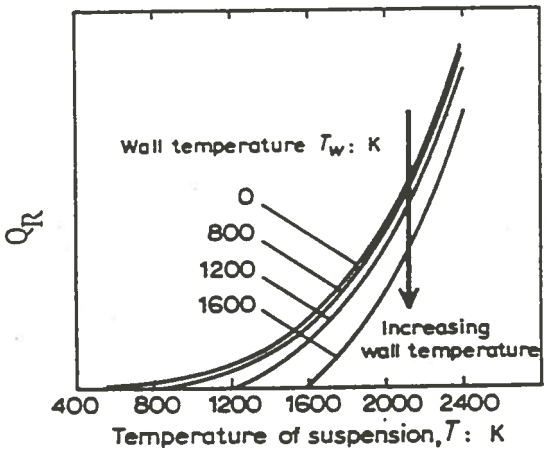

FIGURE 2-5

Heat Removal Rate to the Wall of a Combustion Chamber (Ref. [4])

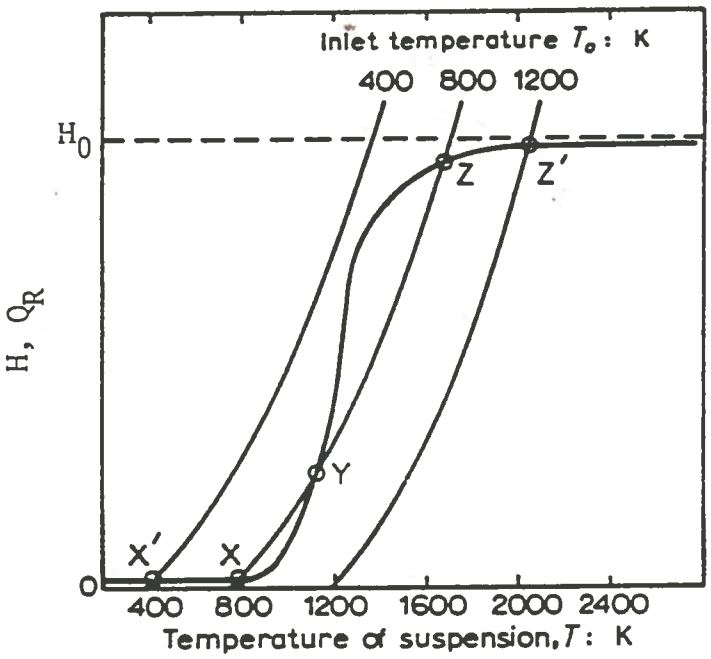

FIGURE 2-6

Superposition of Heat Generation
and Heat Removal Curves (Ref. [4])

This is shown in figure 2-6; three different heat removal rate curves are superimposed on a typical heat generation curve. Depending on the the nature of the heat removal curve, two equilibrium cases are possible

(i) The heat removal curve intersects the heat generation curve at one point only.

This may be further be subdivided into two cases

(a) The point of intersection lies on the limb s1 of the heat generation curve - this represents a stable equilibrium state without ignition, viz. the lower equilibrium temperature,

(b) The point of intersection lies on the limb s3 of the heat generation curve - this represents a stable equilibrium state at the higher temperature indicating that ignition has already occurred.

(ii) The heat removal curve intersects the heat generation curve on all the three limbs s1,s2 and s3. The middle state denotes an unstable equilibrium state and is physically unattainable. A small displacement in the suspension temperature will move the point of intersection to one of the two equilibrium states.

In case (ii), the point X represents the equilibrium state where the amount of combustion is negligible and the temperature is close to the inlet temperature. The point Z represents the equilibrium state where the degree of combustion approaches completion- leading to the onset of ignition. Physically, X and Z correspond to unignited and ignited states respectively. It is the former state which normally occurs in a combustion chamber though a small input of heat source at this point can lead to ignition. The presence of an initial heat source (eg. sensible heat of inlet fuel/air) would normally result in the ignited state.

2B.4 Ignition

As seen in the previous section, ignition occurs when the upper equilibrium state (at the higher temperature) is reached. This state might already exist in the system, or, if the system is in the lower equilibrium state, a small displacement in the equilibrium state will lead to ignition.

When there is only one possible state of equilibrium (cases (i)(a) and (i)(b) in section 2B.3), then a change of state in the suspension (between X′ and Z′ in figure 2-6) can be brought about only by a permanent change in the system. These states X′ and Z′ represent highly stable states since a temporary change in the input conditions (which are subsequently brought back to the initial conditions) will result in a corresponding temporary displacement from the equilibrium and a subsequent return to the original equilibrium state. A permanent change in the system, however, results in a different pair of heat generation-heat removal curves, and leads to the change of state from X′ to Z′ or vice versa, leading to ignition or to the lower equilibrium state respectively.

Contrary to this, when there are two equilibrium states such as X and Z, a temporary change in the input conditions is sufficient to change the equilibrium state. In this case ignition can be achieved by using an independent heat source such as a match or an electric discharge.

CHAPTER III

CROSS-SECTIONS AND INTERACTION COEFFICIENTS

3.1 Radiative properties of polydispersions

It is necessary to know the radiative properties of polydispersions in order to analyze radiative heat transfer in combustion chambers. These properties depend chiefly on the particle size distribution, the refractive index- which varies with the wavelength of radiation and the type of coal, and the spatial distribution of the particles in the chamber. Even if the optical and physical properties of the coal are given, it is often quite difficult and time consuming to determine the exact radiative properties of the particles; hence certain assumptions are made to arrive at these properties.

3.2 Mie theory [8]

In principle, the exact interaction behavior for radiation may be obtained from a rigorous treatment and solution of the Maxwell's electromagnetic wave equations that govern the radiation field for the medium-particle system. The solution however tends to be extremely complicated even for simple particle geometries, and hence in practice, some simplifications are resorted to, one of which is to treat the scattering particles as homogeneous spheres.

This approximation leads to the Mie [8] theory for determining the interaction probabilities. This theory describes the scattered intensity when a plane wave strikes a spherical particle; exact solutions are also available for other regular geometrical shapes, e.g. cylindrical particles. One must bear in mind though that pulverized coal and other

particles in a combustion chamber are neither homogeneous nor perfect spheres. However, it has been shown [1] that Mie theory can be extended to clouds of non-spherical particles of equivalent area since the radiative properties of the cloud are not very much dependent on the exact geometry of the particles. Lee and Tien [16] have recommended the cylindrical shape assumption for the particles.

Mie theory, which is one of the most extensively models used to predict the radiative properties of particles, essentially involves solving the Helmholtz equation by expanding the electric field in an infinite series of eigen functions. In general these are double series and are quite difficult to evaluate. By applying the equations to simple geometries like spheres and long cylinders however, they can be reduced to a single series, thus rendering a solution both feasible [8] and economical using a mainframe computer.

The CALLBH code [8], which applies the Mie theory, yields the spectral scattering and extinction efficiencies Q_η for spherical particles which may then be combined with the particle size distribution characteristics to yield the corresponding interaction coefficient. For a single particle of diameter D this can be represented by [17]

$$\eta_\lambda(\bar{n}_\lambda, N) = Q_\eta(D, \lambda, \bar{n}_\lambda)\ (\pi D^2/4)\ N \qquad 3\text{-}1$$

where η_λ represents any spectral coefficient (absorption κ_λ, extinction β_λ or scatter $\sigma_{s\lambda}$) and Q_η is the corresponding efficiency factor as a function of the size parameter ($\pi D/\lambda$); N is the number density of the particles. All quantities correspond to the wavelength λ. Thus the efficiency factor may be thought of as a ratio between the physical

surface area and the corresponding interaction coefficient of the particle.

For a distribution of particles

$$\eta_\lambda(\bar{n}_\lambda,N) = \int_{D=0}^{\infty} Q_\eta(D,\lambda,\bar{n}_\lambda)\ (\pi D^2/4) f(D)\ N\ d[D] \qquad 3\text{-}2$$

where f(D) represents the size distribution of the particles normalized to unity, viz.

$$\int_{D=0}^{\infty} f(D)\ d[D] = 1 \qquad 3\text{-}3$$

The complex index of refraction is an important optical property required in calculating the radiative characteristics of polydispersions [17]. Though it is quite straight forward to take into account its variation with wavelength, such a treatment is computationally time consuming and hence expensive. In theory, one could incorporate this behavior and formulate the problem. In practice however, these effects may be neglected in order to simplify the treatment [17]; hence it has not been considered in this study.

The other important factor which influences the radiative properties is the size parameter, $\pi D/\lambda$, which is the size of the particle relative to the wavelength of the radiation. Depending on their size parameter, particles may be classified into three categories [8]

(i) Large particles $(\pi D/\lambda > 5)$,

(ii) Small particles $(\pi D/\lambda < 0.6/n)$, and

(iii) Intermediate particles $(0.6/n \leq \pi D/\lambda \leq 5)$

where 'n' is the real part of the complex of index of radiation.

Whereas the "general Mie theory" may be applied to all of the above

cases, it is usually limited to the particles belonging to the intermediate size range (case (ii)). Cases (i) & (ii) are treated as simplifications to the solution of the Maxwell's equations [8].

For the particle size distribution considered in this study, the diameter D ranges from 1 to 70 μm; the wavelength range for the group structure chosen extends from 1 to 30 μm. For an 'n' value of 1.7 (for the coal used in this study), this results in the size parameter ranging from 0.1 to 220; hence the size distribution incorporates particles from all the three classes. Therefore the scatter and absorption coefficients obtained from the application of the general Mie theory would be most suitable for this study.

3.3 Multigroup coefficients

In order to discretize the wavelength variable λ, it is desirable to obtain average interaction coefficients which are constant over the wavelength interval $\Delta\lambda_g$ for group 'g' so that the entire wavelength spectrum of radiation may be divided in to a finite number of energy groups. These interaction coefficients are called group coefficients and have been introduced in chapter II. Various weighting functions are used in radiative transfer studies to integrate the spectral interaction coefficients over the groups. If $f(\lambda)$ represents a typical weighting function, then the group interaction coefficient γ_g for group 'g' bounded by the wavelength limits λ_{gl} and λ_{gu} (the lower and upper group limits) is given by

$$\gamma_g = \frac{\int_{\lambda_{gl}}^{\lambda_{gu}} \gamma(\lambda) f(\lambda)\, d\lambda}{\int_{\lambda_{gl}}^{\lambda_{gu}} f(\lambda)\, d\lambda} \qquad 3\text{-}4$$

where γ_g represents any interaction coefficient (absorption, scatter or extinction) and the weight function $f(\lambda)$ is normalized to unity viz.

$$\int_{\lambda_{gl}}^{\lambda_{gu}} f(\lambda)\, d\lambda = 1 \qquad 3\text{-}5$$

Some of the weighting functions used in radiative transfer and also in this study to collapse the spectral coefficients into discrete group values are

(i) Unit weight function

$$f(\lambda) = 1$$

This gives

$$\gamma_g = \frac{\sum_{i \epsilon g} \gamma_{i+1/2} (\lambda_{i+1} - \lambda_i)}{\sum_{i \epsilon g} (\lambda_{i+1} - \lambda_i)} \qquad 3\text{-}6$$

which represents the numerical integration of the fine point structure within the group 'g' and $\gamma_{i+1/2}$ and $\lambda_{i+1/2}$ are the mean values within the fine structure.

(ii) Planck function [17]

$$f(\lambda) = e_{b\lambda}(\lambda,T) = \frac{2\pi C_1}{\lambda^5 \left[\exp(C_2/\lambda T) - 1\right]}$$

where C_1 and C_2 are constants in Planck's spectral energy distribution with the values

$$C_1 = 0.59544 \times 10^{-16} \text{ W-m}^2 \quad ; \quad C_2 = 14388 \ \mu\text{m-K}$$

Recalling that

$$\int_{\lambda_i}^{\lambda_{i+1}} e_{b\lambda}(\lambda,T)\, d\lambda = (F_{i+1} - F_i)\, \hat{\sigma}T^4 = \Delta F_i\, \hat{\sigma}T^4$$

where

$F_i = F_{0\rightarrow\lambda_i T}$ = black body fraction [13] for λ_i at temperature T

we get

$$\gamma_g = \frac{\sum_{i\epsilon g} \gamma_{i+1/2}\, \Delta F_i}{\sum_{i\epsilon g} \Delta F_i} = \frac{\sum_{i\epsilon g} \gamma_{i+1/2}\, \Delta F_i}{F_g} \qquad 3\text{-}7$$

(iii) Rosseland function [17]

$$f(\lambda) = \frac{de_{b\lambda}(\lambda,T)}{dT}$$

An inverse weighting function is applied with the following definition for the interaction coefficient

$$\gamma_g = \frac{\int_{\Delta\lambda_g} \frac{de_{b\lambda}(\lambda,T)}{dT}\, d\lambda}{\int_{\Delta\lambda_g} \{1/\gamma(\lambda)\} \frac{de_{b\lambda}(\lambda,T)}{dT}\, d\lambda} \qquad 3\text{-}8$$

In the discretized form we get

$$\gamma_g = \frac{\sum_{i\epsilon g} \left\{4F_i - \left[v_{i+1} F'_{i+1} - v_i F'_i\right]\right\}}{\sum_{i\epsilon g} [1/\gamma_{i+1/2}]\left\{4F_i - \left[v_{i+1} F'_{i+1} - v_i F'_i\right]\right\}} \qquad 3\text{-}9$$

where

$$F'_i = \frac{dF_i}{dv} \; ; \quad v = C_2 / \lambda T$$

It is observed here that the group interaction coefficients generated using the Planck and Rosseland weight functions are dependent on the temperature of the medium. Hence, in principle it is necessary to update these coefficients during the computation of the spectral intensity and the temperature for an exact treatment of the problem. This renders the problem more complex as well as more expensive to solve. However it is found that by a judicious choice of the group boundaries, this artificial temperature dependence introduced through the weighting function may be minimized.

3.4 The interaction coefficient data

As mentioned in chapter I, this study assumes a realistic coal sample instead of a mathematical distribution; this is preferable in the analysis and design of combustors and furnaces in order to get a better feel for the order of magnitude of the temperatures and critical

conditions that may be expected in such systems.

The particle size distribution used in this study is one of the three used by Menguc and Viskanta [12]. The sample consists of pulverized lignite coal with a refractive index of 1.7 - 0.066i. The size distribution is presented in table 3-1.

The XSNGEN code has been used to generate the cross-sections and to obtain the extinction and scatter coefficients for the above size distribution. This fine point structure has then been collapsed to give a seven group structure using the code XSN.COLAPS which was developed for this study. These data have been generated using the three weighting functions mentioned in the previous section. The group boundaries have been manipulated to give a group structure with minimal dependence on the temperature; the values have been listed in table 3-2. It is desirable to select a group structure with the minimum number of groups (in order to reduce computational efforts) which will give a good representation of the spectral behavior of the interaction coefficients. With some trial and error, a seven group structure has been found to meet this criterion.

Finally the extinction and scatter coefficients have been determined for a one group structure (table 3-3a) so that the nongray results may be compared with the equivalent one group (gray) results for which the coefficients were calculated using the Planck and the Rosseland weight functions at two temperatures (1000^0 K and 2500^0 K) each and the arithmetic mean of the four values taken to give representative values; this is presented in table 3-3b.

Figure 3-1 shows the spectral variation of the absorption, scatter and extinction coefficients in the wavelength range 1 to 60μm. The

Planck function (normalized with the maximum value of the extinction coefficient) has been overlayed in order to identify the wavelength region of importance for determining the group structure. This is seen to fall in the range $0 < \lambda \leq 30\mu m$. The range selected for this study is $1 \leq \lambda \leq 30\ \mu m$ since the blackbody fraction for $\lambda \leq 1\ \mu m$ at 1000 K is found to be negligible. Figure 3-2 gives the spectral behavior of the interaction coefficients in this range of interest.

The extinction coefficient β_g's for the seven group structure is shown in figure 3-3 for two different temperatures and the three weighting functions (unit, Planck and Rosseland). As discussed earlier, it can be seen that by an appropriate choice of the group boundaries the artificial temperature dependence of the extinction coefficient has been minimized.

TABLE 3-1

Typical size distribution for Pulverized Coal [12]
(Coal density 1300 kg/m , bulk density 0.133 kg/m)

Range (μm)	D_{mi} (μm)	$(w_i/w)/D^3_{mi}$	F_i (%)
1-10	5	4.08E-1	97.66
10-20	15	9.19E-3	2.20
20-40	30	5.56E-4	0.13
40-70	55	1.80E-5	-
70-up	-	-	-

TABLE 3-2

Interaction coefficient data for a 7-group structure
(Planck weight function at 1000 K)

g	λ[μm]	σ_{sg}[1/m]	β_g[1/m]	ω_g	F_g
1	1 - 3	2.5534 E+01	4.7163 E+01	5.4140 E-01	2.7290 E-01
2	3 - 4	3.1309 E+01	5.1956 E+01	6.0261 E-01	2.0763 E-01
3	4 - 6	5.0579 E+01	6.8628 E+01	7.3700 E-01	2.5693 E-01
4	6 - 8	5.0364 E+01	6.5199 E+01	7.7247 E-01	1.1846 E-01
5	8 - 10	3.7899 E+01	5.0191 E+01	7.5510 E-01	5.7908 E-02
6	10 - 15	2.4165 E+01	3.3407 E+01	7.2336 E-01	5.4779 E-02
7	15 - 30	1.3920 E+01	1.9241 E+01	7.2346 E-01	2.6358 E-02

TABLE 3-3a

Interaction coefficient data for a 1-group structure

n	wt. fn.	σ_{sg}[1/m]	β_g[1/m]	ω_g
1	Planck(1000^0 K)	3.6493 E+01	5.4539 E+01	6.6911 E-01
2	Planck(2500^0 K)	2.8048 E+01	4.8858 E+01	5.7406 E-01
3	Ross (1000^0 K)	3.0544 E+01	5.1062 E+01	5.9818 E-01
4	Ross (2500^0 K)	2.5810 E+01	4.7187 E+01	5.4696 E-01

TABLE 3-3b

Mean Interaction coefficient data for a 1-group structure

g	λ[μm]	σ_{sg}[1/m]	β_g[1/m]	ω_g
1	1 - 30	3.0224 E+01	5.0412 E+01	5.9953 E-01

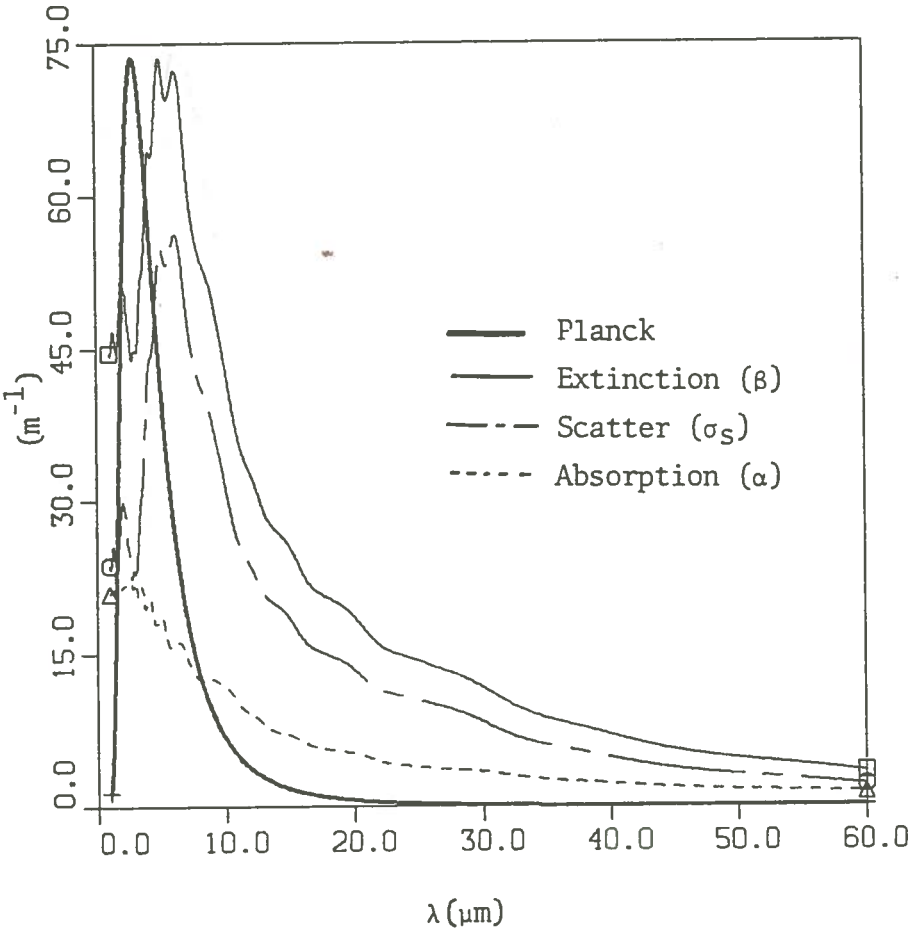

FIGURE 3-1

Spectral Variation of the Interaction Coefficients
($0 < \lambda \leq 60$ μm)

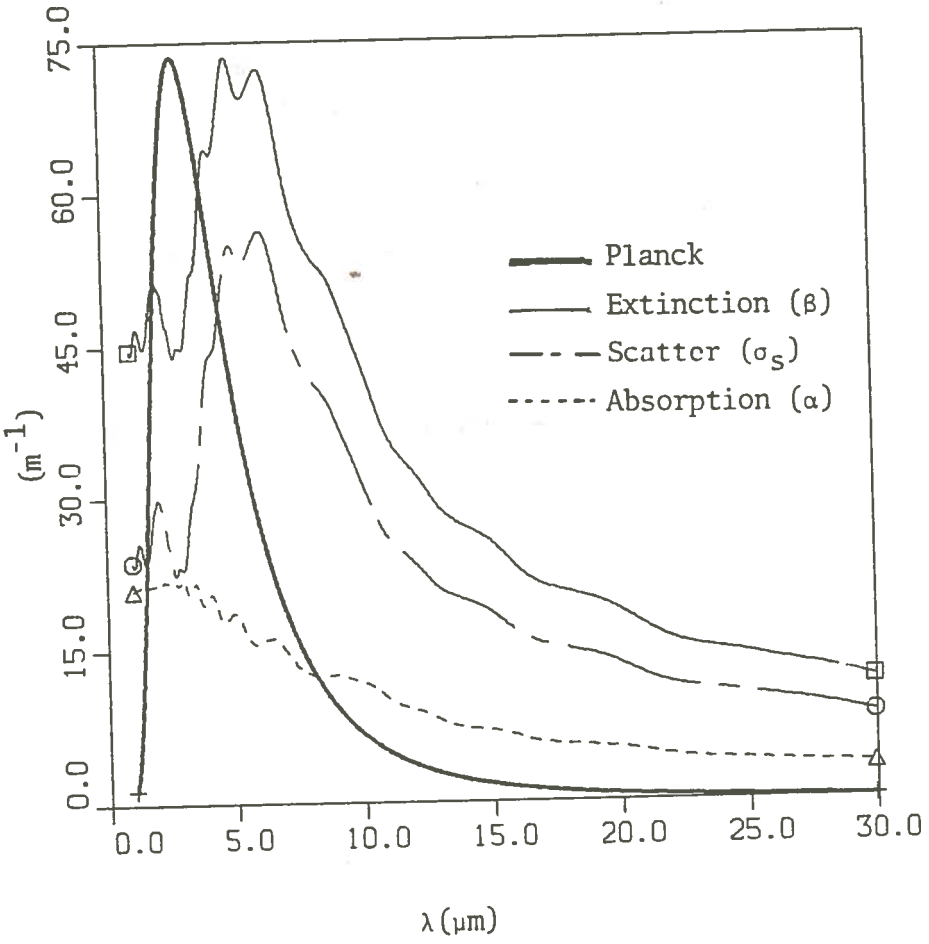

FIGURE 3-2

Spectral Variation of the Interaction Coefficients
($0 < \lambda \leq 30$ μm)

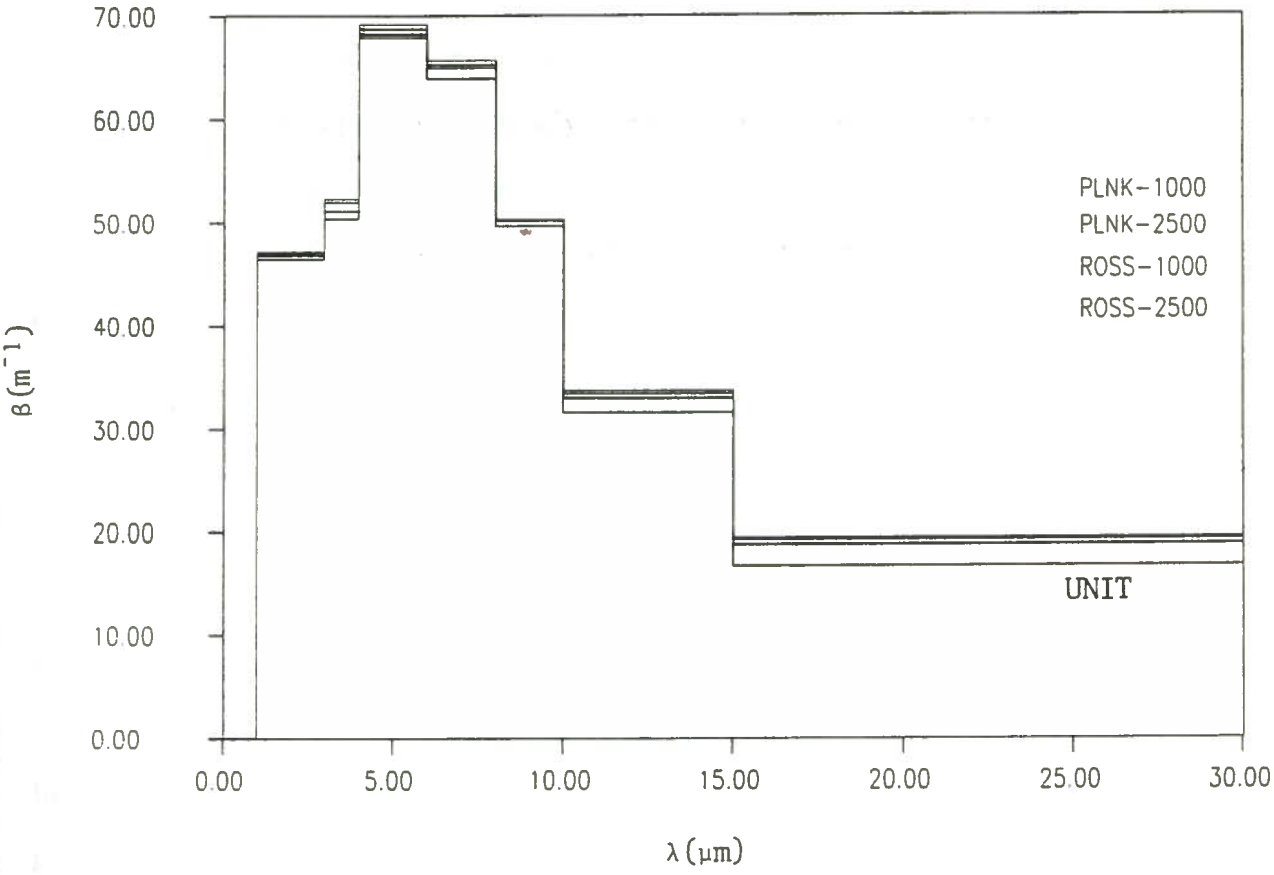

FIGURE 3-3

Multigroup Extinction Coefficient as a Function of λ

CHAPTER IV

RESULTS AND CONCLUSIONS

The FORTRAN code PN3 developed for solving non-linear radiation problems has been applied to study thermal radiation in combustion systems in pulverized coal media. Several test cases have been solved involving gray and nongray media in both planar and cylindrical geometries.

4.1 Planar gray

Gray problems in a planar medium bounded by black walls maintained at a constant unit temperature (dimensionless) have been solved in order to validate the method and to verify the correctness of the code; the results obtained by Crosbie and Pattabongse [3] are taken as reference.

The temperature distribution in the medium has been compared for both uniform heat generation (H = 1.0, α = 0.0) and Arrhenius heat generation (H = 1.0, α = 1.0) in the medium. These results are presented in tables 4-1 and 4-2 respectively for three different optical thicknesses (τ_0). In both problems, the results for all cases compare to within one percent of Crosbie and Pattabongse's. These two sets of results apply to the case of a non-scattering medium (ω = 0.0).

The results obtained in this study with regards to conditions leading to ignition are also found to be compatible with those of Crosbie and Pattabongse. As discussed in chapter II, two equilibrium states in the system are observed for higher values of α. As we move along the lower curve we approach the critical heat generation coefficient H_c, beyond which the lower temperature equilibrium state ceases to exist.

Any further increase in H will cause ignition in the medium with only the high energy solution feasible . Crosbie and Pattabongse [3] have also obtained solutions corresponding to an intermediate equilibrium state for a certain range of $H < H_c$; the actual solution obtained depends on the initial guess for the temperature and the intensity distribution in the medium. This third equilibrium state is highly unstable and can only be obtained within a very limited range of initial guess; it has not been possible to obtain this solution for any of the cases studied in the present work.

The critical heat generation constant H_c (maximum value of H for which a lower temperature solution exists) has been determined for various optical thicknesses τ_0, scattering albedos ω and the exponential factors α. The effects of these parameters on H_c are found to be consistent with those observed by Crosbie and Pattabongse. Increasing the scattering albedo ω is found to decrease the critical heat generation coefficient H_c. This is so because introducing scattering in the medium renders it more difficult for the energy to escape from the medium. A similar effect is noticed when the optical thickness of the system (τ_0) is increased. Thus, ignition occurs at lower energies (H_c) for increasing τ_0 and ω.

Numerical values for H_c for these various cases are given in table 4-3 and compared with those obtained by Crosbie and Pattabongse. The relative difference between the two sets of results is found to vary between 0.28 percent for $\alpha = 10.0$, $\tau_0 = 1.0$, $\omega = 0.9$ and 33.4 percent for $\alpha = 10.0$, $\tau_0 = 10.0$, $\omega = 0.0$. In general the values of H_c are found to agree within 5-10 percent.

The method of solution employed by Crosbie and Pattabongse is exact whereas the P_3 method adopted in this study is an approximation to the third order. This is one possible cause of discrepancy in the two sets of results. The second and more important cause could be the fact that there is no definite criterion to define an exact value for the critical heat generation H_c. As may be seen from the 'S' curves, this value is reached very gradually and it becomes increasingly difficult to obtain the solution for the lower temperature as the value of H_c is approached. Hence the determination of H_c depends on the iteration parameters and the incremental value of H; it may be mentioned here that though the value of H_c varies somewhat, the corresponding difference in the temperatures is observed to be minimal.

4.2 Planar nongray

The seven group and the one group interaction coefficients generated with the size distribution used by Menguc and Viskanta [12] have been used to study the effect of treating a nongray problem as an equivalent gray problem; a comparison is made of the results obtained from using these two group structures.

Two geometrical lengths 2L = 0.1 m and 0.2 m have been considered. These correspond to optical thicknesses of 6.86 and 13.72 in the seven group model (based on the maximum group extinction coefficient) and to 5.04 and 10.08 in the one group model respectively.

The temperature distribution in planar systems with black walls maintained at a constant dimensionless temperature of 1.0 is shown in figure 4-1. The maximum temperature for all cases is found to occur at the center; this is as expected since the system is symmetric about the

center, thus causing an equivalent reflected boundary condition about the midplane. This symmetry is apparent from the temperature distribution curves. The temperatures correspond to the lower equilibrium state for various α's with 2L = 0.1 m and H = 10.0. The temperatures obtained from the seven group model are found to be higher than those obtained using the one group model for all cases, though both models tend to give a more or less flat distribution for large α's. Since the seven group structure is a more detailed and accurate representation of the interaction coefficients, it may be deduced that the equivalent gray model tends to underestimate the temperatures in the system.

The relative difference in the maximum temperature between the two models is found to be 11.48 percent for α = 1.0, 18.51 percent for α = 5.0 and 0.73 percent for α = 8.0. The small difference for α = 8.0 is because of the fact that the heat generation term becomes very small with increasing α, thus resulting in a flat temperature distribution in the medium, with all temperatures being close to the wall temperature.

As discussed in the previous section, increasing H leads to a discontinuous jump in the temperature; this multi-solution behaviour for the seven group model, for various values of α, is shown in figures 4-2 and 4-3. The curves are observed to be continuous for small values of α; the characteristic 'S' curves are observed for higher values of α. For these cases the upper level temperature solution is obtained by starting at a large value of H and moving towards smaller values of H. The opposite of this viz. starting with a value of H less than H_c and increasing H in subsequent steps, is not possible. Similarly, in order to obtain the lower equilibrium temperatures, convergence is achieved by

starting with a small value of H and moving along the positive H axis.

It can be observed from the above figures the that greater the value of the dimensionless activation energy α, the more abrupt the jump from the lower to the higher equilibrium state or in other words, the more pronounced the ignition effect.

The critical heat generation coefficient H_c determined using the gray and nongray models are tabulated in table 4-4. The results for 2L = 0.1 m and 0.2 m and for α = 8.0, 9.0 and 10.0 are presented. The relative difference in the values of H_c using the two models is found to vary between 35.67 percent for 2L = 0.2 m, α = 8.0 and 38.48 percent for 2L = 0.1 m, α = 10.0. The corresponding S-curves for the two models have been compared in figure 4-4. It is observed that for a given value of α, the seven group nongray model requires a lower energy (H_c) to induce ignition. The rise in the temperature however is found to be larger for the multi-group case thus indicating a "stronger" ignition process for the nongray model. Also, the value of H_c is found to be consistently lower for increasing optical thickness τ since more energy gets trapped within the suspension for higher τ.

Finally, the surface radiative heat flux (at z = 2L) has been plotted vs. H in figure 4-5 for the multi-group model. Curves are presented for three different values of α. The behavior of the surface heat flux is found to be similar to the surface temperature variation (figures 4-2 and 4-3). The curves are continuous for α values lower than a critical value (7.0-8.0). Multi-solution behavior is observed for α = 8.0. The non-gray model is found to give higher estimates for the surface heat fluxes as compared to the equivalent gray model.

4.3 Cylindrical nongray

The problems solved for the planar nongray model have been repeated in the cylindrical geometry using the same interaction coefficients; similar tables and figures have been generated.

The temperature distribution for the lower equilibrium state in the medium for the two models with R = 0.1 m, H = 10.0 and for different values of α, have been compared in figure 4-6. Once again the one group structure is found to underestimate the temperatures in the medium. The relative difference in the maximum temperature between the two models is found to be 11.85 percent for α = 1.0, 17.81 percent for α = 5.0 and 1.17 percent for α = 8.0. Again, the small value for this difference at α = 8.0 is due to the flattening of the temperature distribution in the medium at this large value of α.

A slight shift in the maximum temperature is observed to cause a dip in the center. This results from the P_3 approximation to the radiative transfer equation.

Figures 4-7 and 4-8 show the multi-solution behavior for radial dimension of 0.1 m and 0.2 m respectively for the seven group model; the curves depict this behaviour for various α's.

Table 4-5 compares the critical heat generation coefficient H_c given by the seven group structure and the equivalent one group structure. Two radial dimensions 0.1 m and 0.2 m corresponding to optical thicknesses of 6.86 and 13.72 in the seven group model and 5.04 and 10.08 in the one group model respectively are considered. The three α's considered are α = 8.0,9.0 and 10.0. The relatively difference in H_c between the two models is found to vary from 37.17 percent for R = 0.2 m, α = 8.0 and

38.48 percent for R = 0.1 m and α = 10.0.

The 'S' curves for the two models with α = 10.0 are shown in figure 4-9; the curves are presented for R = 0.1 m and 0.2 m As in the planar case, the one group structure is found to overestimate the critical heat generation coefficient H_c and shift the curves to the right.

The surface heat flux (at r = R) variation is compared for the gray and nongray models in figure 4-10. The variation is compatible with that observed in the slab model. Multi-solution behavior is seen only for the case where α = 8.0. Again the nongray model predicts higher values for the surface heat fluxes.

The multi-solution behavior is observed in both planar and cylindrical systems in both gray and nongray media whenever the value of the exponential factor 'α' is greater than a critical value. It is interesting to note that this value seems to lie between 7.0 and 8.0 for all cases regardless of the geometry of the system, the optical properties (interaction coefficients) of the medium or the geometrical dimension of the system. Prior studies [3] have found this value to be around 7.5.

4.4 Conclusions

The methodology and the computer code developed here may be applied to various non-linear radiation problems with a temperature dependent heat generation in the system. In comparing the results for pulverized coal combustion problems, it is meaningful to compare temperatures and intensities in the medium. However, in order to compare asymptotic values such as the critical heat generation coefficient H_c, one would have to come up with standard criteria to determine the value to a

certain degree of accuracy.

The computer runs for the nongray problems have mostly been run on the IBM 3084; some of the cases were run on the IBM 3090 super computer. The installation of the new super computer motivates further research in this and related areas.

TABLE 4-1

Temperature distribution for uniform heat generation (H=1.0, α=0.0, ω=0.0)

τ/τ_0	$\theta(\tau)$ present method	$\theta(\tau)$ Crosbie	rel diff.(%)
τ_0=0.1			
0.0000000	1.2081	1.2131	- 0.412
0.1182402	1.2085	1.2160	- 0.617
0.2896810	1.2090	1.2180	- 0.739
0.5000000	1.2091	1.2187	- 0.788
τ_0=1.0			
0.0000000	1.3285	1.3234	+ 0.385
0.1182402	1.3543	1.3622	- 0.580
0.2896810	1.3766	1.3874	- 0.778
0.5000000	1.3871	1.3970	- 0.709
τ_0=10.0			
0.0000000	1.8334	1.8148	+ 1.025
0.1182402	2.3140	2.3168	- 0.121
0.2896810	2.5821	2.5847	- 0.101
0.5000000	2.6687	2.6800	- 0.422

TABLE 4-2

Temperature distribution for Arrhenius heat generation (H=1.0, α=1.0, ω=0.0)

τ/τ_0	$\theta(\tau)$ present method	$\theta(\tau)$ Crosbie	rel diff.(%)
τ_0=0.1			
0.0000000	1.0982	1.1011	- 0.263
0.1182402	1.0984	1.1028	- 0.399
0.2896810	1.0987	1.1040	- 0.480
0.5000000	1.0988	1.1044	- 0.507
τ_0=1.0			
0.0000000	1.1760	1.1729	+ 0.264
0.1182402	1.1889	1.1988	- 0.826
0.2896810	1.2080	1.2159	- 0.650
0.5000000	1.2153	1.2226	- 0.597
τ_0=10.0			
0.0000000	1.6507	1.6347	+ 0.979
0.1182402	2.0776	2.0806	- 0.144
0.2896810	2.3048	2.3231	- 0.788
0.5000000	2.3988	2.4099	- 0.461

TABLE 4-3

Critical heat generation coefficients for planar gray problems

α	τ_0	ω	H_c present method	H_c Crosbie	rel diff.(%)
8.0	1.0	0.0	337.20	334.00	+ 0.96
8.0	2.0	0.0	172.90	188.90	- 8.47
9.0	1.0	0.0	753.50	738.00	+ 2.10
9.0	2.0	0.0	385.90	419.60	- 8.03
9.0	10.0	0.0	31.17	46.00	- 32.24
10.0	0.1	0.0	3985.00	3763.00	+ 5.90
10.0	1.0	0.0	1761.00	1708.00	+ 3.10
10.0	2.0	0.0	892.00	970.00	- 8.04
10.0	5.0	0.0	240.50	320.00	- 24.84
10.0	10.0	0.0	71.00	107.00	- 33.64
10.0	1.0	0.2	1603.00	1560.00	+ 2.76
10.0	1.0	0.5	1262.80	1237.00	+ 2.09
10.0	1.0	0.8	683.00	677.40	+ 0.83
10.0	1.0	0.9	387.30	386.20	+ 0.28
10.0	5.0	0.2	237.30	314.80	- 24.62
10.0	5.0	0.5	228.00	299.00	- 23.75
10.0	5.0	0.8	197.50	249.00	- 20.68
10.0	5.0	0.9	161.40	194.70	- 17.10

TABLE 4-5

Comparison of H_c for 7-group and 1-group models (cylindrical)

	H_c		
α	7 group	1 group	rel. diff.(%)
R_0=0.1			
8.0	30.80	42.30	+ 37.33
9.0	68.50	94.50	+ 37.90
10.0	158.00	218.80	+ 38.48
R_0=0.2			
8.0	9.70	13.30	+ 37.17
9.0	21.60	29.70	+ 37.50
10.0	49.90	68.80	+ 37.88

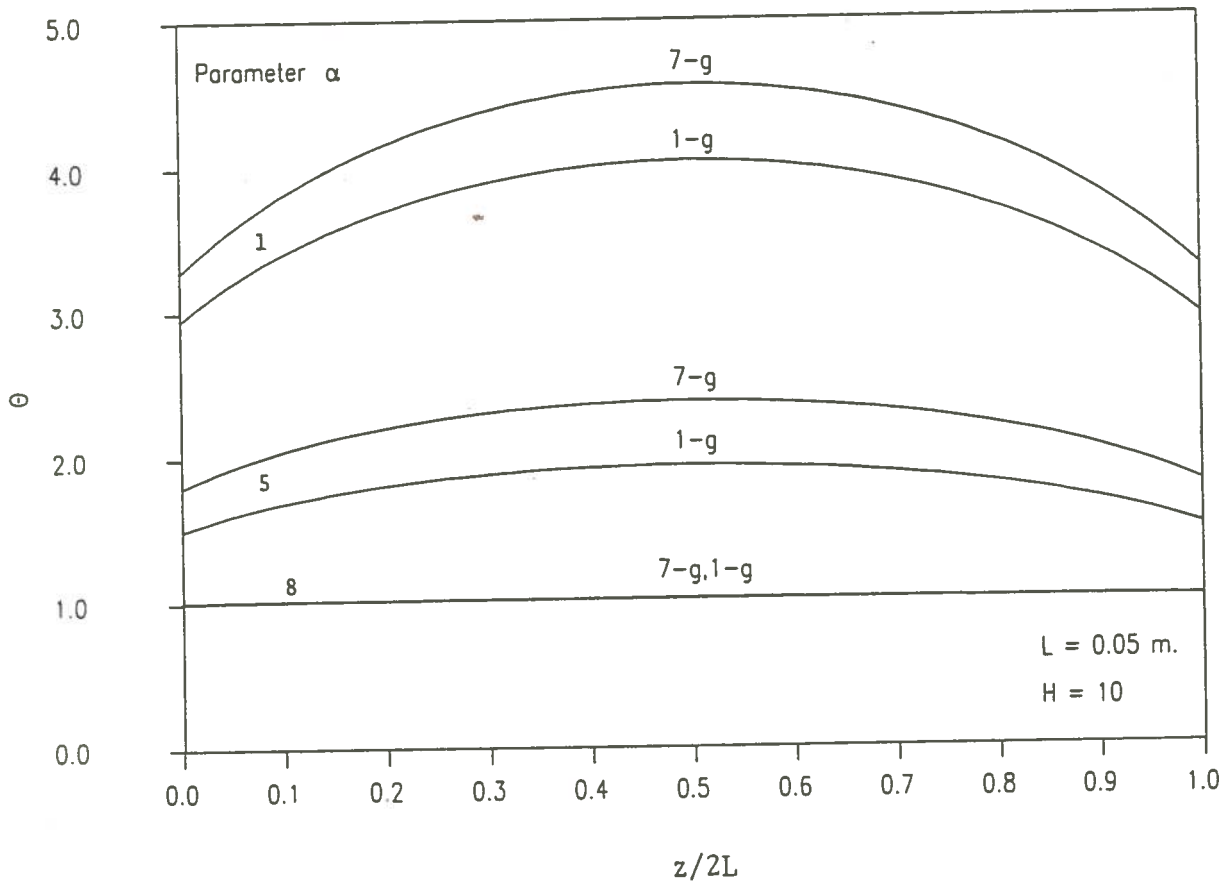

FIGURE 4-1

Temperature Distribution in a Slab (Seven Groups)

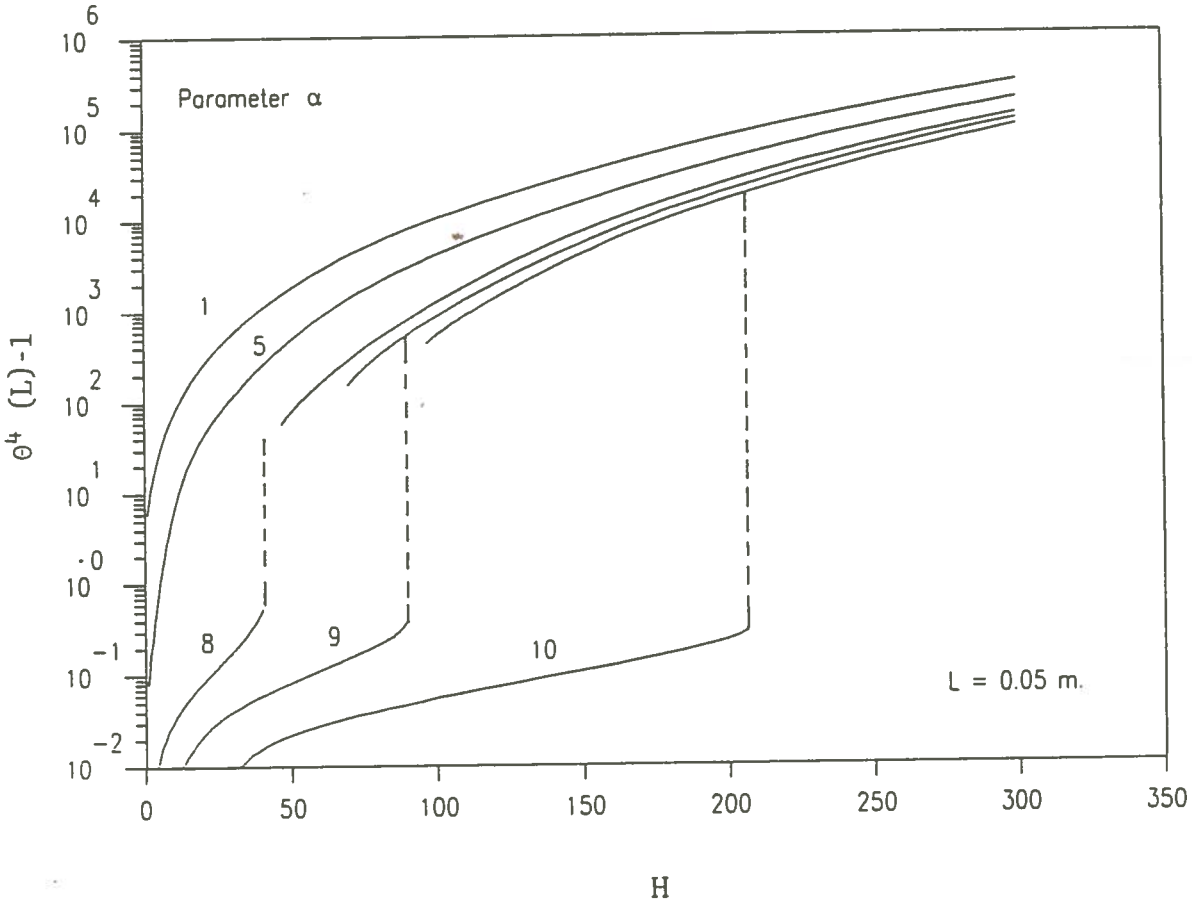

FIGURE 4-2

Multi-Solution Temperature Behavior in a Slab (Seven Groups)

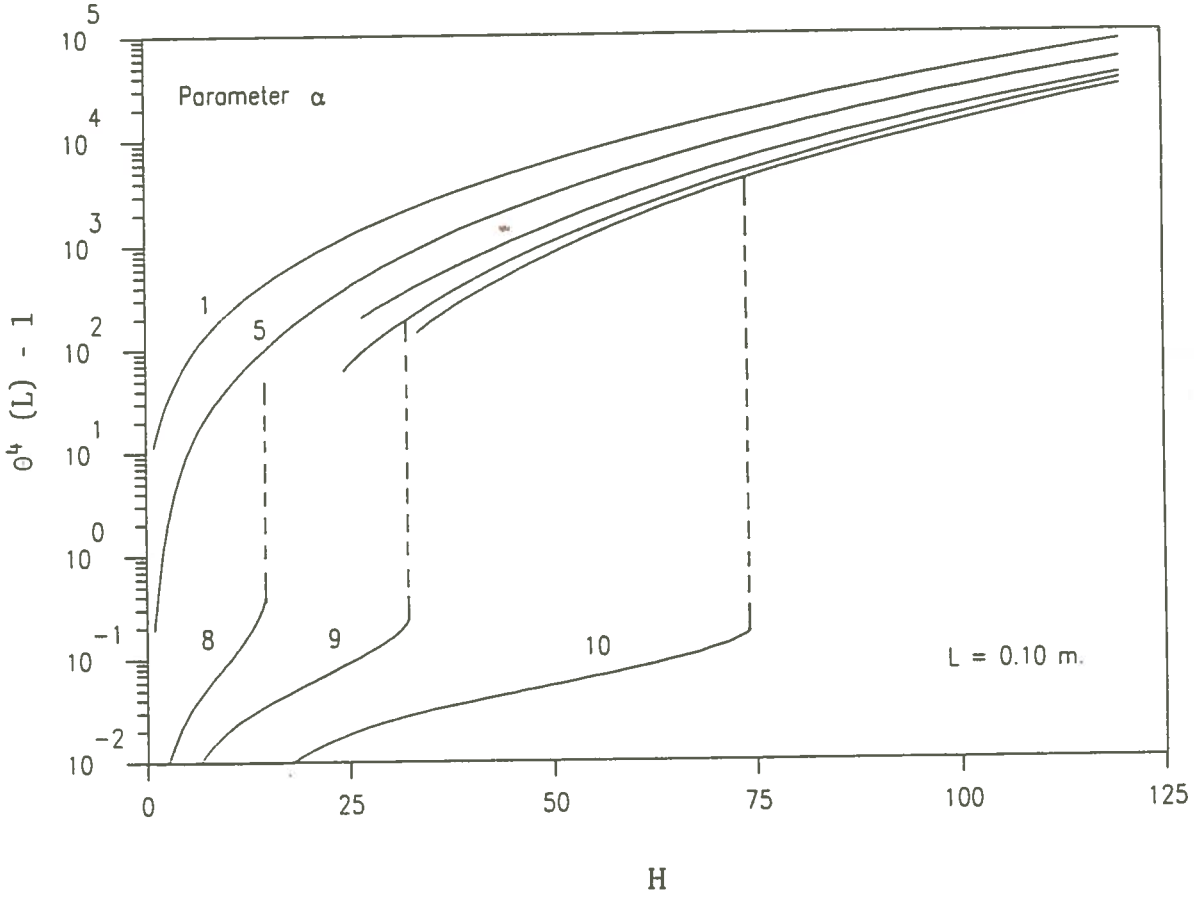

FIGURE 4-3

Multi-Solution Temperature Behavior in a Slab (Seven Groups)

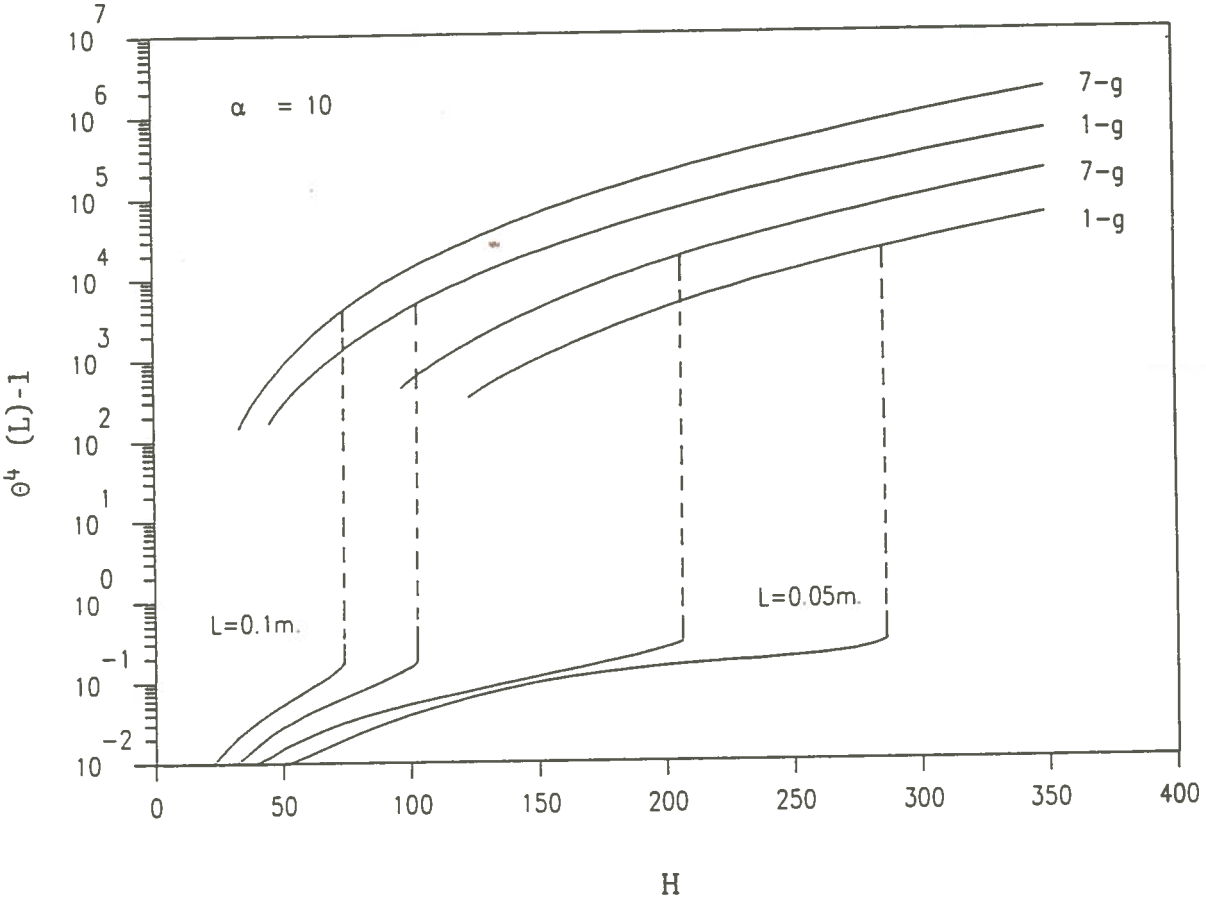

FIGURE 4-4

Influence of Group Structure on Multi-Solution Behavior (Slab)

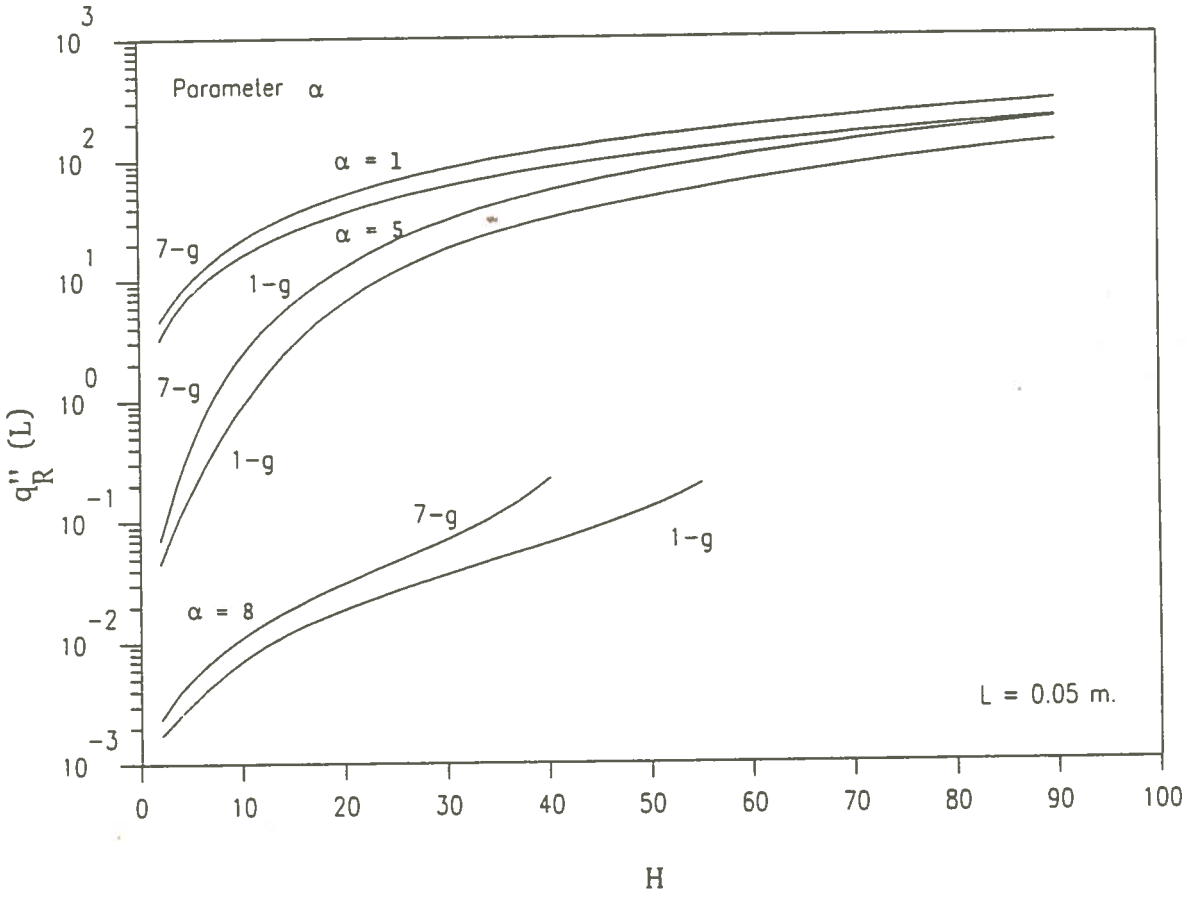

FIGURE 4-5

Influence of Group Structure on Surface Heat Flux (Slab)

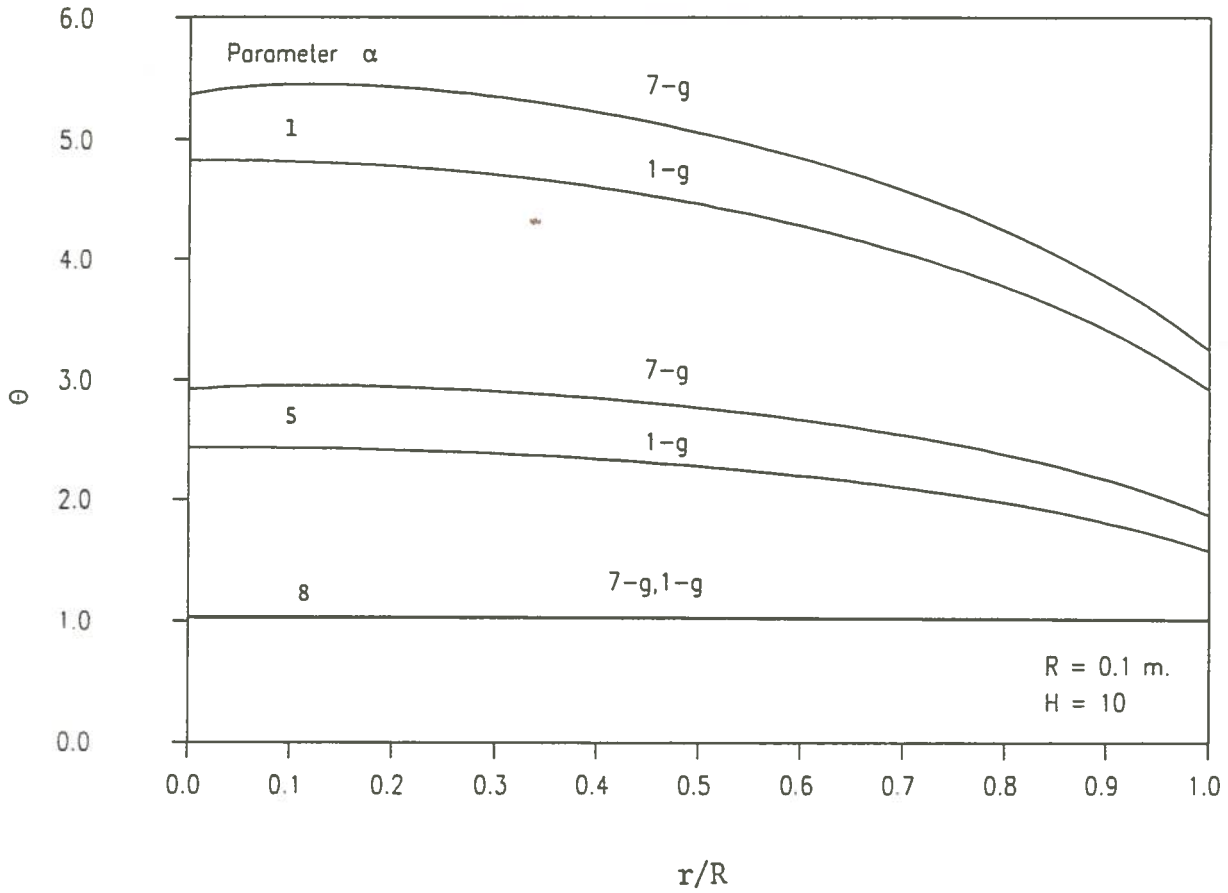

FIGURE 4-6

Temperature Distribution in a Cylindrical Medium (Seven Groups)

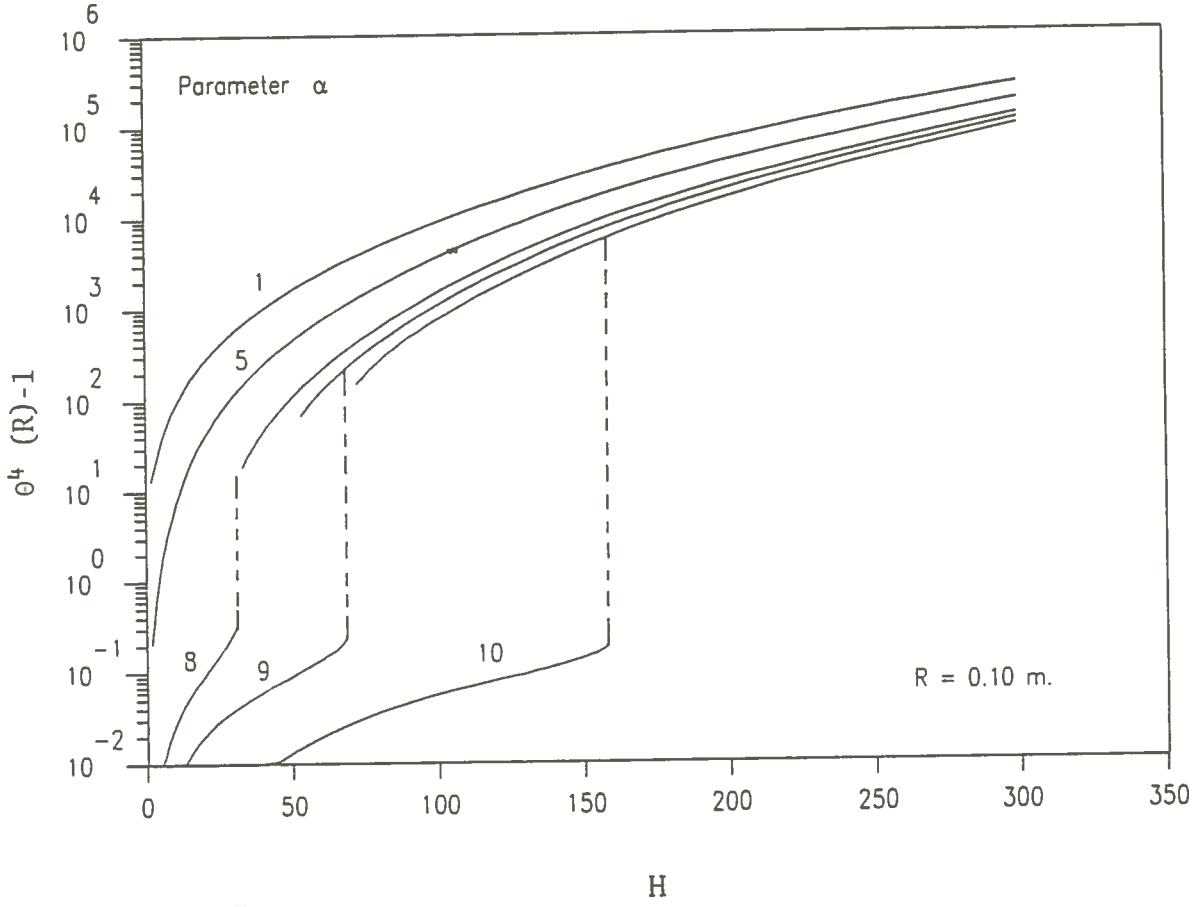

FIGURE 4-7

Multi-Solution Behavior in a Cylindrical Medium (Seven Groups)

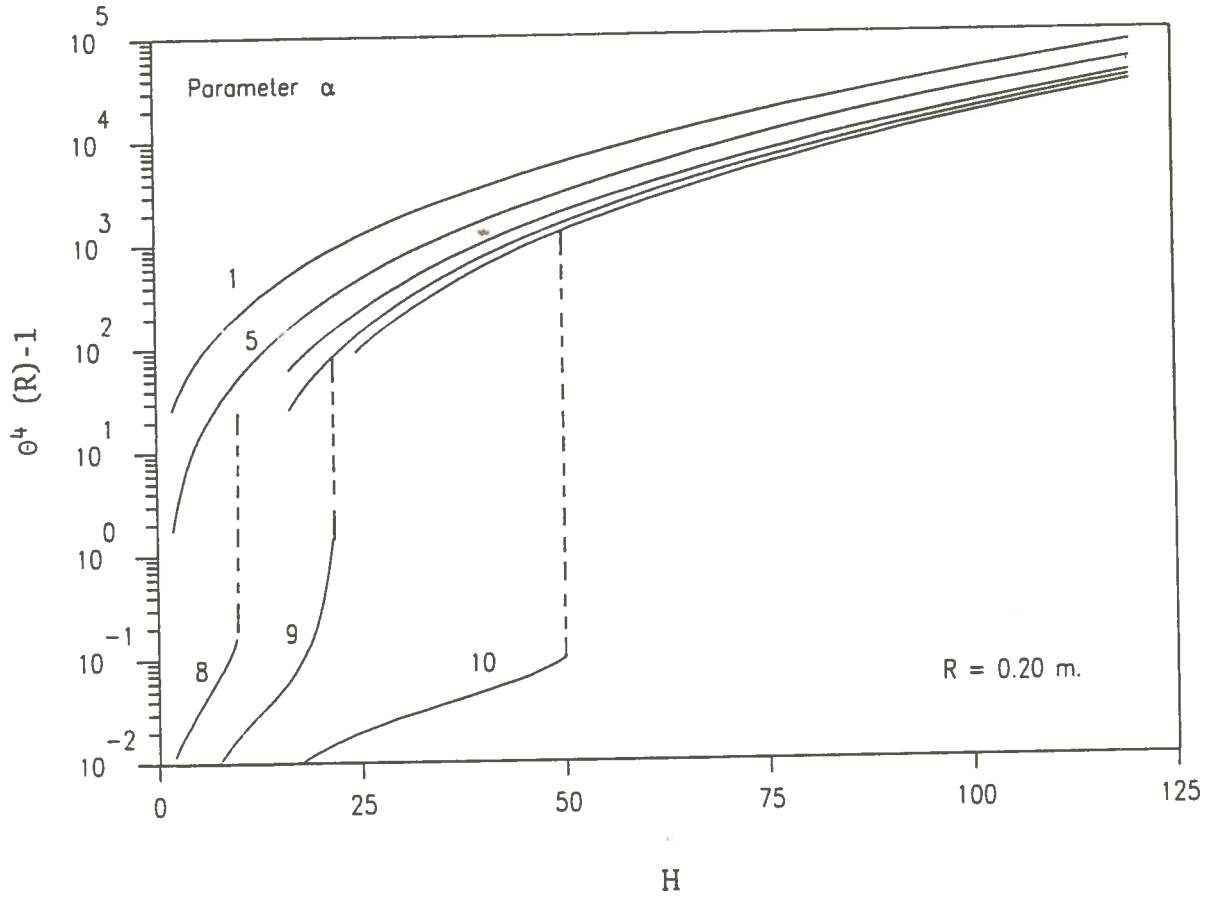

FIGURE 4-8

Multi-Solution Behavior in a Cylindrical Medium (Seven Groups)

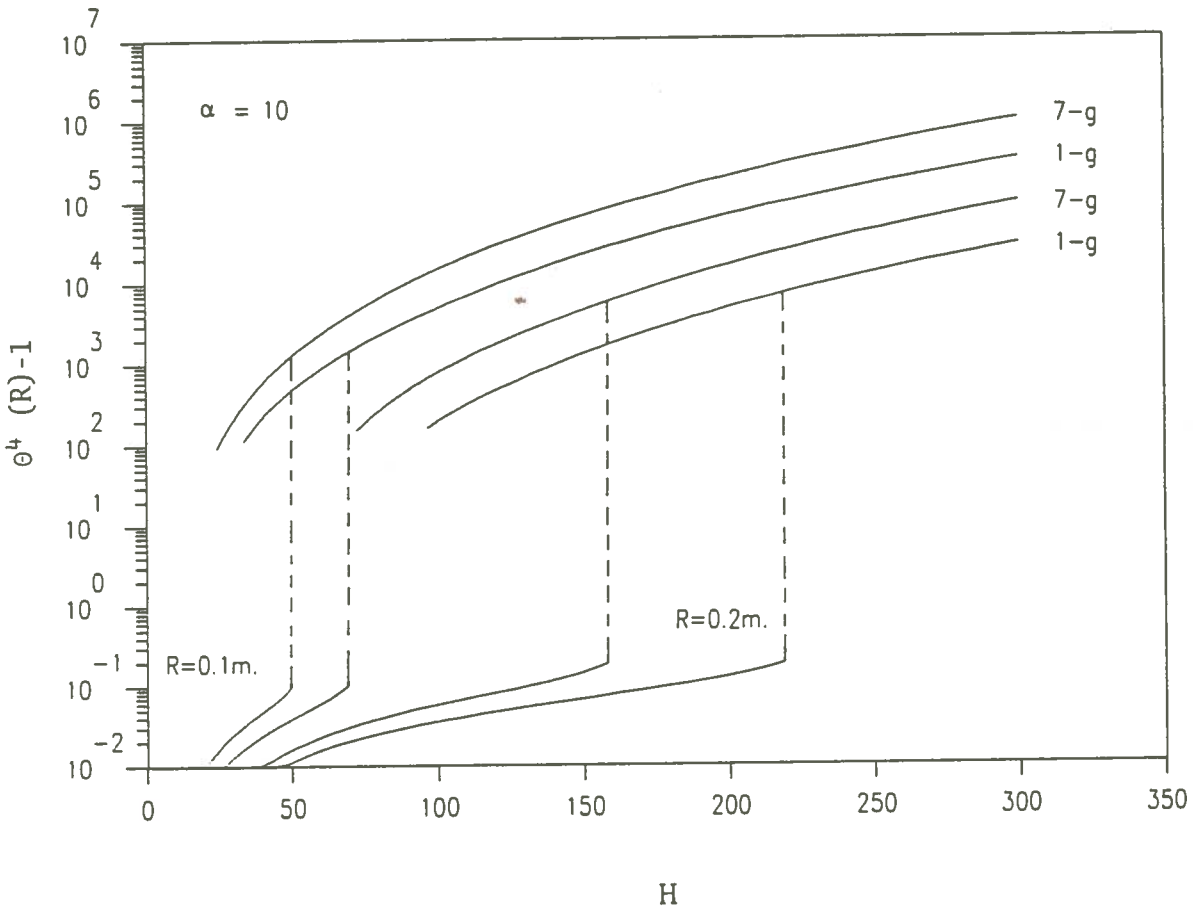

FIGURE 4-9

Influence of Group Structure on Multi-Solution Behavior
(Cylindrical)

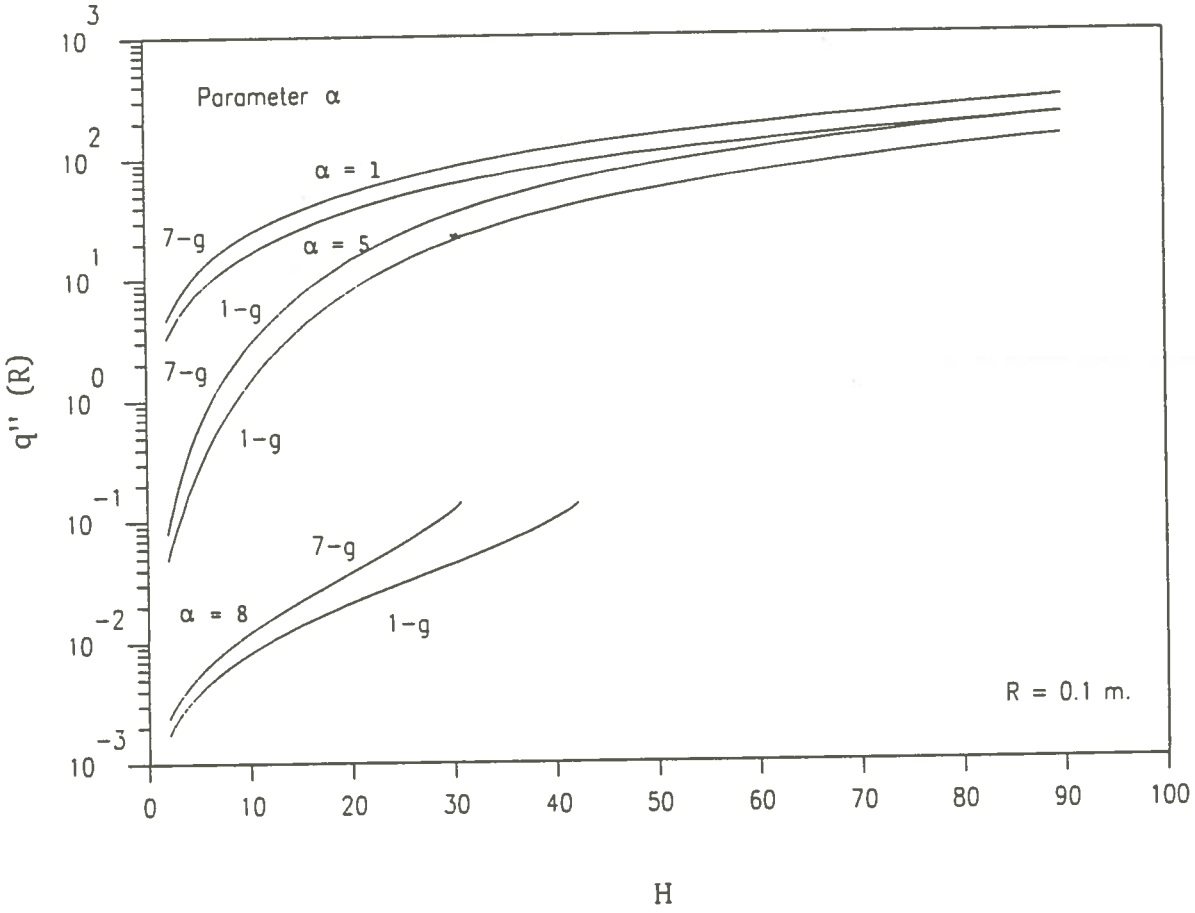

FIGURE 4-10

Influence of Group Structure on Surface Heat Flux (Cylindrical)

REFERENCES

1. R. Viskanta and M.P. Menguc, Radiation heat transfer in combustion systems, *Prog. Energy Combust Sci.*, Vol. 13, 1987.

2. H. Khalil et al., Stationary thermal ignition of particle suspensions, *J. of Heat Transfer*, Vol. 105, May 1983.

3. A.L. Crosbie and M. Pattabongse, Radiative ignition in a planar medium, *J. Quant. Spectrosc. Radiat. Transfer*, Vol. 37, 1987.

4. M.A. Field et al., *Combustion of pulverized coal*, The British Coal Utilization Research Association, Surrey, England(1967).

5. P. Gray and P.R. Lee, Thermal Explosion Theory, *Oxidation and Combustion Reviews*, 1967, Vol. 2, Elsevier, Amsterdam.

6. R.H. Essenhigh and J. Csaba, The thermal radiation theory for plane flame propogation in coal dust clouds, *Ninth International Symposium on Combustion*, 1963, Academic Press, New York.

7. V.S. Arpaci and R.J. Tabaczynski, Radiation-Affected Laminar Flame Propogation, *Combustion and Flame*, 1982.

8. C.F. Bohren and D.R. Huffman, *Absorption and Scattering of Light by Small Particles*, Wiley & Sons publications, 1983.

9. H. Khalil et al., Ignition of Particle Suspensions by Radiant Emission from Bounding Walls, *Combustion and Flame*, 53: 149-152

(1983).

10. A.L. Crosbie and M. Pattabongse, Transient Conductive Transfer in a Planar Layer with Arrhenius Heat Generation, *J. Quant. spectrosc. Radiat. Transfer*, 1987, Vol. 37.

11. H. Khalil, Radiative transfer in pulverized coal suspensions, M.S. thesis, Kansas State Univ., Kansas (1978).

12. M.P. Menguc and R. Viskanta, A Sensitivity Analysis for Radiative Heat Transfer in a Pulverized Coal-Fired Furnace, *Comb. Sci. and Tech.*, 1987. Vol. 51, pp. 51-74.

13. R. Siegel and J.R. Howell, *Thermal Radiation Heat Transfer*, Hemisphere Publishing Corp., New York, 1981.

14. A. Yucel and Y. Bayazitoglu, P-N Approximation for Radiative Heat Transfer in a Nongray medium, AIAA Journal, Vol. 21, No. 8.

15. J. Higenyi, Higher order differential approximation of radiative energy transfer in a cylindrical gray medium, Ph.D. thesis, Rice University, Houston, Texas (1979)

16. S.C. Lee and C.L. Tien, Effect of Soot Shape on Soot Radiation, *J. Quant. Spectrosc. Radiat. Transfer*, Vol. 29, 1981, pp. 259.

17. M.P. Menguc and R. Viskanta, On the Radiative Properties of Polydispersions: A Simplified Approach, *Comb. Sci. and Tech.*, 1985. Vol.44, pp. 143-159.

18. A. Yucel, H. Kehtarnavaz, and Y. Bayazitoglu, Interaction of Radiation with the Boundary Layer: Nongray Media, *ASME*, 83-HT-33

19. A. Miele, S. Naqvi and A.V. Levy, Modified Quasilinearization Method for Solving Nonlinear Equations, *Aero-Astronautics Report*, No. 78, Rice University, 1970.

APPENDIX A

Numerical method of solution to the system of equations

There are various numerical schemes available to solve the system of equations derived in chapter II using the P-3 approximation. The method used in this study is known as the collocation method [18]. The method essentially consists of discretizing the spatial variable into a finite number of mesh intervals and approximating the dependent variable (temperature and intensity moments in our case) by Hermite polynomials within each interval; The cubic Hermite polynomials are used in this study and are given by

$$H_i^0(s) = 1 - 3s^2 + 2s^3$$
$$H_i^1(s) = h_i(s - 2s^2 + s^3)$$
$$H_{i+1}^0(s) = 3s^2 - 2s^3$$
$$H_{i+1}^1(s) = h_i(s^3 - s^2)$$

where

$h_i = \tau_{i+1} - \tau_i$ = mesh spacing between nodes i and i+1

$s(\tau) = (\tau - \tau_i)/h_i$ = relative distance within interval i

and τ is the optical length.

The temperature θ and the intensity moments I_{0g} and I_{2g} within a mesh interval 'i' are approximated in terms of the node values of the functions and their derivatives to give

$$\theta_i(\tau) = \theta(\tau_i)H_i^0(\tau) + D\theta(\tau_i)H_i^1(\tau) + \theta(\tau_{i+1})H_{i+1}^0(\tau) + D\theta(\tau_{i+1})H_{i+1}^1(\tau)$$

$$I_{0i}(\tau) = I_0(\tau_i)H_i^0(\tau) + DI_0(\tau_i)H_i^1(\tau) + I_0(\tau_{i+1})H_{i+1}^0(\tau) + DI_0(\tau_{i+1})H_{i+1}^1(\tau)$$

$$I_{2i}(\tau) = I_2(\tau_i)H_i^0(\tau) + DI_2(\tau_i)H_i^1(\tau) + I_2(\tau_{i+1})H_{i+1}^0(\tau) + DI_2(\tau_{i+1})H_{i+1}^1(\tau)$$

The above equations are forced to satisfy the equations at two collocation points given by Gaussian quadrature within each interval

$$\tau_{i1} = \tau_i + \xi_1 h_i \quad ; \quad \tau_{i2} = \tau_i + \xi_2 h_i$$

where

$$\xi_1 = 1/2 - 1/\sqrt{12} \quad \text{and} \quad \xi_2 = 1/2 + 1/\sqrt{12}$$

Thus for IM intervals (IM+1 nodes) and IGM groups we get 2(1 + 2*IGM)*IM equations. We also have 2(1 + 2*IGM) from the two sets of boundary conditions thus giving a total of 2(1 + 2*IGM)*(IM + 1) equations. Since we have (IM + 1) nodes, the number of unknowns is also 2(1 + 2*IGM)*(IM + 1); we thus have consistent system of equations.

For our seven group structure (IGM = 7) we have 2(1 + 14) = 30 equations per mesh interval and 30 boundary conditions.

These equations when cast into a matrix, resulted in a banded matrix with both lower and upper diagonals and a band width of 30. The number of mesh intervals chosen was 20 (21 mesh points). Increasing the number of intervals to 50 was found to have no effect on the results. The MQA algorithm [19] was used to solve the system of non-linear equations. The maximum number of iterations and the maximum number of bisections were set to 30 and 15 respectively. The smallest increment in H adopted was 0.1. For values of H not near H_c, convergence was generally obtained within 30 iterations and the CPU time taken on the IBM 3090 was in the order of seconds for the planar case and in the order of a minute for the cylindrical case. In the vicinity of H_c, both the number of iterations required and the CPU time increased to higher values.

Vita

J. Sundar was born in Madras, India on August 11, 1962 to S. Jambunathan and J. Bagyalakshmi. He attended the Kendriya Vidyalaya, Central School in Madras and New Delhi and graduated in 1980.

He received his B. Tech in civil engineering from the Indian Institute of Technology, Madras - India in December 1984. He entered graduate school at Louisiana State University in 1985 in the department of Nuclear Engineering.